Unravelling biological processess and EGFR pathway regulation by the receptor-like protein tyrosine phosphatase PTPRH in non-small cell lung cancer

Mylena M. O. Ortiz[1,2], Deeya M. Patel[3], Matthew Swiatnicki[2], and Eran R. Andrechek[2,4]

1 – Genetics and Genomic Sciences Program

2 - Department of Physiology

3 - Lyman Briggs College

4 – Contributing Author

Eran R. Andrechek

Department of Physiology

Michigan State University

2194 BPS Building

567 Wilson Road

East Lansing, MI

48824

andrech1@msu.edu

(517)884-5020

Authors' contributions

MO and DP performed all experiments, MS contributed to the experimental design, MO and ERA contributed to the experimental design and drafting of the manuscript.

Abstract

The delicate balance of protein phosphorylation is often disrupted in cancers, with hyperactivity of kinases and inactivation of phosphatases driving cell proliferation and survival pathways. PTPRH, a receptor-like protein tyrosine, is deregulated or mutated in certain cancers, including non-small cell lung cancer (NSCLC). However, the biological processes that PTPRH is involved in and how they may contribute to tumorigenesis are unknown. Previous studies have linked PTPRH to the regulation of the EGFR pathway but the full extension of this regulation and the underlying mechanisms remain to be elucidated. We found that PTPRH knockout in NSCLC cells tends to increase the phosphorylation levels of EGFR at the tyrosine residue 1173 (1197), whereas overexpression of PTPRH wild-type significantly decreases phosphorylation. Surprisingly, disruption of the extracellular or intracellular domains of the phosphatase leads to EGFR dephosphorylation in a similar manner. Co-immunoprecipitation and proximity-dependent biotinylation (BioID) experiments demonstrated that PTPRH do not directly interact with EGFR, but rather with NF-κB, a transcription factor downstream of the EGFR pathway. Besides NF-κB, BioID revealed 48 novel PTPRH interactors in NSCLC cells, with the strongest associations observed for PTPRH itself, HELZ2, and RFC2. Moreover, we report for the first time that PTPRH is primarily involved in translation and RNA-associated pathways. Guided by RNA sequencing analysis, we observed that overexpression of the phosphatase downregulates multiple oncogenic signature pathways and modulates the gene expression of 34 protein tyrosine phosphatases and 45 tyrosine kinases, EGFR included. Together, these results shed light on the importance of PTPRH in regulating biological and cellular processes and how its inactivation may support cancer progression.

Introduction

Phosphorylation and dephosphorylation are key post-translational modifications that intricately regulate cell signaling cascades[1]. In normal cells, these two events are tightly regulated in time and space by kinases and phosphatases and together they orchestrate fundamental cellular processes, such as proliferation, differentiation, and apoptosis[2,3]. However, this delicate equilibrium is often disrupted in multiple diseases, notably cancers[4]. The hyperactivation of kinases and inactivation of phosphatases leads to aberrant cell proliferation, migration, and survival, thereby supporting cancer initiation, progression, and resistance to therapies[5].

In non-small cell lung cancers (NSCLC), activating mutations in the receptor tyrosine kinase (RTK) *EGFR* are observed in approximately 50% of patients from Asian inheritance and 20% in Caucasians[6]. The vast majority are in-frame deletions, point mutations, or insertions in the first few exons of the EGFR kinase domain (exons 18-21), such as the classical L858R substitution and exon 19 deletion[7–9]. These mutations result in ligand-independent activation of the EGFR pathway by stabilizing EGFR dimers in an active conformation[10,11]. Subsequential transphosphorylation of tyrosine residues in the C-terminal tail of EGFR recruits signaling molecules and activates the downstream pathways including PI3K/mTOR/Akt, RAS/RAF/MEK/ERK, and IL-6/JAK/STAT3[12–14]. Therefore, these mutations are generally responsive to EGFR inhibitors (EGFRi), when not combined with resistance mutations due to hyperactivity of the RTK. In addition to *EGFR*, other oncogenic kinases are also found to be frequently mutated in NSCLC, including *PIK3CA* (~13%), *SKT11* (~12%), *MET* (~7%), *ALK* (~7%), *BRAF* (~6%), *HER2* (~6%), *ROS* (~5%), *RET* (~4.5%), *AKT1* (~2%), and *MAP2K1* (~1%)[15–17]. Many of these kinases activate similar downstream pathways to EGFR and are actionable drug targets[18].

Mutations in phosphatases and their consequences, on the other hand, are much less well understood. While kinases generally act as oncogenes, phosphatases can exhibit characteristics of either tumor suppressors or oncogenes in lung cancers[19]. A well-known example is *PTEN*, an important tumor-suppressor gene mutated in approximately 7% of NSCLC cases. The inactivation of this phosphatase leads to an increase in the PI3K/mTOR/Akt signaling pathway and lower survival rates[20,21]. Conversely, activating mutations in the tyrosine phosphatase *PTPN11*/Shp2 increases phospho-ERK 1/2 levels and activates the MAPK pathway, thus behaving as an oncogene[22]. More recently, our group has shown that point mutations in the receptor-like protein tyrosine phosphatase (RPTP) *PTPRH* are observed in 6% of NSCLC patients and over 80% of MMTV-*PyMT* mice, a murine model of breast cancer[23,24]. Mutation that results in inactivation of this phosphatase leads to elevated phosphorylation of EGFR at tyrosine 1173 (alternatively numbered as 1197) and results in activation of the Akt pathway[23–25]. This suggests that

PTPRH contributes to negatively regulating the EGFR pathway; nonetheless, the precise underlying mechanism is unclear.

PTPRH, also known as SAP-1, is a transmembrane protein and part of the tyrosine phosphatase family, which encompasses over 100 members[26]. Structurally, PTPRH is composed of an extracellular region rich in fibronectin type 3 (FN3) repeats, a hydrophobic transmembrane domain, and a single intracellular phosphatase domain[27,28]. Little is known about PTPRH kinetics and interactors; however, a few associations with tyrosine kinase signaling and cellular processes have been found in different cell types. By dephosphorylating tyrosine residues, PTPRH is suggested to negatively regulate T-cell function[29], intestinal immunity[30], integrin-associated pathways[31], and, more recently, EGFR signaling[23–25,32]. Furthermore, PTPRH has been found to induce apoptotic cell death pathways[33] and to stimulate c-Src activity[34].

The participation of this phosphatase in cancer, although not fully elucidated, seems to be largely related to the tissue of origin. PTPRH expression varies across and within different cancer types and conflicting findings are observed[27,35–37]. For instance, in colorectal cancers, PTPRH plays a causal role in cancer progression, but not initiation, and overexpression is observed in some cases[29,38]. On the other hand, as hepatocarcinoma advances to poorly differentiated stages, a decrease in the phosphatase level is observed[39]. In lung cancers, *PTPRH* mutations happen in ~6% of the patients, and *PTPRH* and *EGFR* mutations were found to be mutually exclusive[23]. Therefore, it is evident that we do not understand the full spectrum of cell signaling regulation by PTPRH and how it stimulates or suppresses tumorigenesis. To bridge this gap, we built a comprehensive map of PTPRH interactors and associated cell signaling networks. We started to investigate the mechanisms by which PTPRH regulates the EGFR pathway by assessing the physical interaction between the two proteins and the ability of different PTPRH constructs to dephosphorylate the kinase in NSCLC cell lines. Following this, we expanded our search to cover all proteins and signaling pathways regulated by the phosphatase. To achieve this, we used a comprehensive protein-protein interaction assay, tandem mass spectrometry (MS/MS), and RNA sequencing. Our study revealed novel PTPRH interactors and functions, shedding light on the role of this phosphatase in the cellular context of lung cancers.

Results

Investigation of EGFR phosphorylation status in lung cancer cells in the absence of PTPRH

As PTPRH is a protein tyrosine phosphatase and published observations suggest that it regulates EGFR signaling[23–25], we, therefore, investigated how the inactivation of PTPRH affects EGFR phosphorylation status in lung cancer. We hypothesized that PTPRH negatively regulates EGFR; thus, phospho-EGFR levels (pEGFR) would increase in the absence of the phosphatase. To confirm this relationship, we used our previously generated human lung adenocarcinoma cell line NCI-H23 *PTPRH* knockout (H23 KO), whose parental cell line is wild-type for *PTPRH* and *EGFR*. Previous data from our lab suggests that PTPRH affects phosphorylation of the EGFR tyrosine residue 1173 (pEGFR 1173, also known as pEGFR 1197), we first screened pEGFR 1173 levels in two knockout clones following EGF stimulation for 15 min. Although densitometry of the western blot bands revealed approximately a two-fold increase in one of the clones (H23 KO#13) when pEGFR 1173 was corrected by the total EGFR levels, none of them presented a significant change compared to the parental cells although a trend was evident (Supplementary Fig. 1D).

Since EGFR phosphorylation and activation happen rapidly after ligand binding and dimerization[40,41], we reasoned that an increase in pEGFR1173 in H23 PTPRH KO cells could reach a maximum at other time points following EGF stimulation. To test this, we stimulated the parental and knockout cells with EGF for 5, 15, 30, 60, and 120 minutes. As demonstrated in Fig. 1B, the 15-minute time point presents the biggest difference in pEGFR1173/total EGFR ratios between the two groups. However, concordant with our initial observations, none of the time points were statistically significant although an increasing trend was evident. Concomitantly, we also evaluated the activation of one of the downstream EGFR pathways, the AKT pathway. Following EGF stimulation, the phospho-AKT increases gradually and reaches maximum activation in both groups around the 30-minute time-point, but no difference in pAKT/total AKT ratios was seen between the H23 and H23 KO groups within the same time point.

We then began to consider whether PTPRH might dephosphorylate a tyrosine residue other than 1173. To investigate potential differences in phosphorylation at other EGFR tyrosine residues between the groups, we immunoprecipitated EGFR from both H23 and H23 PTPRH KO cells stimulated with EGF for 15 minutes, and quantified phospho-tyrosine residues using tandem mass spectrometry (MS/MS). Our

analysis revealed that two tyrosine residues, Y1086 and Y1173, were phosphorylated in most replicates from both groups (see Fig. 1C). Consistent with our western blot findings, H23 PTPRH KO cells exhibited an approximately two-fold increase in pEGFR1173 levels; however, the differences in phosphorylation levels of Y1086 and Y1173 did not quite reach significance. Notably, phosphorylation of Y992 and Y1068 was detected exclusively in the knockout cells, but only in 1 out of 3 replicates. Together, these results demonstrate a trend to increase pEGFR 1173 levels in lung adenocarcinoma cells when PTPRH is absent.

Investigation of EGFR phosphorylation status in lung cancer cells overexpressing PTPRH wild-type or various deletions

Considering that we did not see significant changes in pEGFR when using the *PTPRH* knockout cells, we reasoned that one explanation could be the low PTPRH protein levels in the parental cells (Supplemental Fig. 1A-B). To address this issue, we took the opposite strategy and stably overexpressed PTPRH wild type (WT) containing a C-terminal HA tag in the H23 KO cells. In addition to WT, we also generated different groups of cells overexpressing various *PTPRH* in-frame deletions in different domains of the protein. The purpose of this approach was to investigate how these deletions altered PTPRH regulation of EGFR phosphorylation status. Since the extracellular portion of PTPRH is composed of multiple fibronectin 3 (FN3) domains, we started by deleting blocks of two consecutive FN3 (constructs Δ1-3) using site-directed mutagenesis. The intracellular catalytic site of the phosphatase domain was deleted in the Δ4 construct. A schematic of the deletions is presented in Fig. 2A. We were unable to generate an *in-frame* deletion of the last FN3 domain due to the repetitive sequences situated in the extracellular portion of the phosphatase. To validate the successful generation of our constructs, we sequenced their *PTPRH* regions and aligned the sequences against the human *PTPRH* WT coding sequence. All constructs contained in-frame deletions in the desired region (Fig. 2B). We also noticed the presence of a synonymous mutation across all constructs (c.717 G>C). Moreover, as a consequence of the site-directed mutagenesis method, a mutation was introduced in the c.1157 C>A position of Δ1 construct, resulting in the P386H substitution despite multiple attempts to revert it to the wild-type. Immunoblot using antibodies against PTPRH and the HA tag revealed similar banding patterns between the two blots, but different sizes of bands across the addback groups, confirming the overexpression on the various PTPRH deletions (Fig. 2C).

Given that we demonstrated maximal phosphorylation at 15 minutes after EGF stimulation in Figure 1, we used this time point to collect lysates from cells expressing the various PTPRH constructs. As anticipated, while the H23 PTPRH KO group tended to increase pEGFR 1173 compared to H23 cells, the difference was not statistically significant. However, as expected upon overexpression of PTPRH WT

addback in the PTPRH knockout line, a significant decrease of approximately 2-fold was observed (Fig. 2C). The pEGFR levels in the various deletion addbacks were then compared to the wild-type addback. Surprisingly, all PTPRH deletions yielded similar results to the wild-type addback, even the one lacking the catalytic site. Consequently, it seems that neither the FN3 domains nor the catalytic site of PTPRH are necessary for EGFR Y1173 dephosphorylation. Taken together, these findings suggest a role for PTPRH in regulating EGFR, though further investigation is required to fully understand the underlying mechanism.

Evaluation of protein-protein interaction between PTPRH and EGFR

To further clarify whether PTPRH directly interacts with EGFR and regulates tyrosine kinase signaling, we conducted a protein-protein interaction experiment using co-immunoprecipitation (Co-IP). For this purpose, we stimulated H23 parental cells with EGF for 15 minutes, followed by immunoprecipitation of EGFR and immunoblot for EGFR and PTPRH. H23 PTPRH KO cells were used as a negative Co-IP control, whereas whole-cell lysates (WCL) from the colorectal adenocarcinoma cell line HT-29, known to express PTPRH at elevated levels[37], were used as a positive control for immunoblotting. As demonstrated in Fig. 3A (top panel), a substantial amount of EGFR was recovered from all cell lines, however, PTPRH co-immunoprecipitation was not observed (bottom panel).

To overcome the difficulties associated with low PTPRH protein levels in the H23 cells or the possibility of a transient interaction between the two proteins, we repeated the experiment using our previously generated cell line in which wild-type PTPRH was added back to the H23 PTPRH knockout cells and overexpressed. Protein lysates were collected at 2, 5, 10, and 15 min post-EGF stimulation. Despite varying EGF stimulation, PTPRH was not observed in the immunoprecipitated fraction (Fig. 3B). Together, these results demonstrate that PTPRH does not directly interact with EGFR in any of the time points in a manner detectable by co-IP. . This raises several possibilities, including that either PTPRH-EGFR interactions may happen rapidly following EGFR phosphorylation or that other proteins or phosphatases are involved in EGFR dephosphorylation.

BioID reveals novel PTPRH interactors in lung cancer cells

Based on the results that EGFR phosphorylation was regulated in an unknown mechanism by PTPRH, we next wanted to establish this mechanistic association between the two. Considering that little is known about PTPRH interaction partners and how this phosphatase may regulate different biological processes, we explored those interactions through a comprehensive protein-protein interaction assay. We used BioID2 for this purpose, an *in-vitro* labeling technique that adds a biotin tag to proteins interacting stably or transiently with the protein of interest in a labeling radius of ~10 nm[42]. BioID2 followed by an HA tag

was cloned into the C-terminal of the PTPRH wild-type coding sequence, in proximity to its intracellular phosphatase domain. Two different lung adenocarcinoma cell lines (NCI-H2023 and H23 PTPRH KO) were infected with lentiviruses containing wild-type PTPRH-BioID2 or BioID2-only, the latter being a control to assess non-specific biotinylation. To validate the expression of the constructs, an immunoblot against the HA tag was performed. All the cell lines infected with BioID2-only or wild-type PTPRH-BioID2 presented bands at the expected molecular weight, while no bands were seen in the mock lanes (Fig. 4A). We then performed immunofluorescence using antibodies against HA (Fig. 4B) and BioID2 (Supplementary Fig. 2) to evaluate whether the BioID2 tag would affect PTPRH subcellular localization. While BioID2 is highly expressed in the cytoplasm and nucleus of the BioID2-only cells, the modified PTPRH was found to be expressed at lower levels in the plasma membrane and cytoplasm, in agreement with the subcellular localization of the endogenous counterpart.

We hypothesized that PTPRH regulates different cell signaling pathways, including those emanating from other tyrosine kinases. To begin to test this, all groups of cells were serum-starved for 24 hours, followed by FBS stimulation with a complete medium supplemented with biotin for 18 hours. Immunoblot against biotin in the WCL revealed promiscuous biotinylation in the cells infected with BioID2-only (Fig. 5A). Importantly, some biotinylated proteins showed up exclusively in the wild-type PTPRH-BioID2 group, suggesting that these proteins are specifically interacting with PTPRH. Biotinylation was not observed in the mock group, validating the activity of the BioID2 enzyme and the experimental results.

Biotinylated proteins were immunoprecipitated, followed by their identification using MS/MS. When analyzed individually, H2023 and H23 PTPRH knockout cells expressing wild-type PTPRH-BioID2 revealed a total of 90 and 130 candidate interactors, respectively (Fig. 5B, and Additional File 1 and 2). These candidate interactors exhibited at least a 3-fold increase in wild-type PTPRH-BioID2 cells compared to their corresponding BioID2-only cells. To ensure reproducibility, we selected proteins detected in both cell lines, with a minimum +3-fold change in the wild-type PTPRH -BioID2 group compared to BioID2-only. This filtering step resulted in 48 proteins that met the criteria and the list of PTPRH candidate interactors is in Table 1. The top 3 potential interacting proteins were PTPRH itself (31,000-fold change), followed by the helicase HELZ2 (14,000-fold change), the replication factor RFC2 (9,500-fold change), and NFKB2 (5,800-fold change). Considering that receptor tyrosine kinase phosphatases, PTPRH included, are thought to form dimers, this data suggests that PTPRH can be found as a homodimer in our infected cells[34,43].

Since the proposed role for PTPRH is to dephosphorylate tyrosine residues, we then evaluated how many proteins from this list are reported to have at least one phospho-site in the PhosphoSitePlus database. 88.6% (n=43) of PTPRH candidate interactors are reported to have at least one phospho-tyrosine site and

100% (n=48) present at least one phospho-serine or phospho-threonine site (Fig. 5C). We then sought to understand whether the candidate proteins interact with each other and form complexes of biological relevance. STRING analysis revealed several interacting proteins forming one major network and four smaller ones (Fig. 5D). To elucidate the biological processes associated with these proteins, we conducted a DAVID functional annotation analysis, and subsequently reported annotations with a significant threshold of $p < 0.05$ after multi-hypothesis correction (Table 2). Despite our initial hypothesis that PTPRH regulates tyrosine kinase pathways, we found an enrichment of biological processes related to translation and RNA binding. Post-translational modifications related to phosphoproteins were also significant as expected; however, we have also observed enrichment of Ubl conjugation, acetylation, and isopeptide bond. In summary, these results highlight PTPRH's participation in novel biological pathways, raising the possibility that PTPRH also accumulates non-canonical roles.

Transcriptome analysis of lung cancer cells overexpressing PTPRH

To further validate our BioID2 results and gain a deeper understanding of PTPRH participation in biological pathways and cancer, we generated two NSCLC cell lines overexpressing wild-type PTPRH (H23 PTPRH overexpression and H2023 PTPRH overexpression), followed by RNA-sequencing. We also included the parental cells (endogenous PTPRH expression) and H23 PTPRH knockout cells in our analysis. We followed similar conditions to the BioID2 experiment: cells were serum starved for 24 hours and stimulated with FBS in complete medium for 16 hours before RNA extraction. Principal component analysis (PCA) of the normalized reads shows that cells cluster primarily based on the PTPRH status (PC1- 82% variance): parental cells cluster on the right, while PTPRH overexpressing cell lines on the left (Fig. 6A). PC2 reflects 9% of the variance and further separate the clusters based on the transcriptome of the original cell type (H2023 vs H23 derived cells). Surprisingly, the H23 PTPRH knockout cells cluster closely to the H23 PTPRH overexpression cells, which is also evidenced by our clustering analysis (Supplementary Fig. 3A and Fig. 6C). We believe that this reflects a drift of phenotype caused by the ablation of PTPRH after a few passages.

Differential expression analysis demonstrated that 1,360 genes present over a 2-fold increase (upregulated genes) and 2,060 genes present over a 2-fold decrease (downregulated genes) in a significant manner in PTPRH overexpressing cells compared to parental cells (Fig. 6B, Supplementary Fig. 3C, and Additional File 3). These represent PTPRH signature genes and the top 30 genes up and downregulated are shown in Fig. 6C. The most upregulated genes are SERPINB2 (13.76 fold increase), a protein shown to inhibit migration and to increase the resolution of inflammation[44], the retrotransposon-derived gene RTL1 (13.25 fold increase), the transcription factor ERG (12.87 fold increase), and cyclin D2 (12.21 fold increase). Among the most downregulated genes are the cadherin CDH17 (19.9 fold decrease), AGR2 (19.38 fold

decrease), which participates in protein folding and has been shown to be involved in cancer progression[45], and CYP4F11, a member of the cytochrome P450 family.

To understand how the differentially expressed genes (DEG) modulated by PTPRH are involved in biological pathways and cancer, we performed pathway enrichment analyses using GO and Molecular Signature (MSigDB) databases. Our gene set enrichment analysis (GSEA) using the oncogenic signature C6 revealed multiple significantly downregulated pathways in the cell lines overexpressing PTPRH, including NFE2L2, MEK, LEF1, E2F1, KRAS, RAF, P53, ERBB2, and others (Fig. 6G). We have also observed significant downregulation of genes involved in the EGFR (NES = - 1.55) and AKT (NES = - 1.53) pathways, in agreement with our hypothesis and previous findings that PTPRH negatively regulates EGFR and downstream signaling pathways (Fig. 6H and Supplementary Fig. 3B). The hallmark MSigDB showed downregulation of gene sets involved in estrogen response, interferon alpha and gamma responses, reactive oxygen species, IL6-JAK-STAT3 signaling, and metabolism (adipogenesis, xenobiotic, and fatty acid metabolism), and upregulation of proliferation pathways (E2F targets, G2M checkpoint) and the WNT-Beta-catenin signaling (Fig. 6F). Concordant with or BioID results, pathway enrichment analysis using GO biological processes gene sets showed significant upregulation RNA splicing and ribonucleoprotein biogenesis (Table 3). Furthermore, DNA repair, chromosome organization and chromatin remodeling pathways were also positively enriched, whereas fatty acid and monocarboxylic acid metabolism were shown to be downregulated.

We next asked whether PTPRH overexpression would modulate the expression of other protein tyrosine phosphatases (PTPs) and tyrosine kinases (TKs). We interrogated our RNA-seq data based on the genes that were present in our DEG analysis and found that 34 PTPs (Fig. 6D) and 45 TKs (Fig. 6E) were differentially expressed in the PTPRH overexpressing cell lines. Overall, 24 PTPs were downregulated, suggesting redundancy in function among the PTPs. The PTPs showing the strongest downregulation were PTPN20, PTPRQ, PTPRVP, PTPRJ, PTPRM, PTPRN, and PRPRU, whereas PTPRD, PTPRR, PTPRH itself, PTPN2, and PTPRB were the most upregulated ones. Interestingly, the majority of TKs presented increased gene expression levels (n = 28) and some were found to be downregulated (n= 17), including EGFR. Among the TKs with the strongest upregulation are FLT3, EPHB1, KIT, ROR2, NTRK1, PDGFRA, EPHB6, and EPHA7. On the other hand, MST1R, EPHA8, ERBB3, LMTK3, TEK, ROR1, FGFR1, and PDGFRB were the most downregulated TKs. Collectively, these results reinforce that PTPRH modulates not only TKs but also PTPs, and participates in multiple oncogenic pathways and biological processes previously unknown.

Discussion

Little is known about the role of the receptor-like protein tyrosine phosphatase PTPRH in the regulation of various cell signaling pathways and how alterations may contribute to tumorigenesis. To address this gap of knowledge, we investigated PTPRH's candidate interactors and the participation of this phosphatase in biological and cellular processes in two NSCLC cell lines, in addition to its influence on the EGFR pathway. We were able to find novel protein-protein interactions and cell signaling pathways in which PTPRH is involved and a connection between EGFR signaling and PTPRH was demonstrated in our RNA-sequencing results and pEGFR screening. Moreover, we report for the first time that this receptor-like protein tyrosine phosphatase is involved in RNA binding and processing, ribosome biogenesis, metabolism, and cell division-related pathways.

By assessing pEGFR sites in the absence of PTPRH or overexpression of various PTPRH constructs, our findings suggest that PTPRH may regulate EGFR phosphorylation status at tyrosine 1173 (1197) position but this regulation is not direct, as demonstrated by our Co-IP and BioID experiments. We observed that, although not significant, H23 PTPRH KO cells tend to have higher pEGFR 1173 (1197), whereas rescuing wild-type PTPRH expression in H23 PTPRH knockout significantly decreases the phosphorylation of EGFR tyrosine 1173 (1197). Concordantly, MS/MS revealed no consistent changes in phosphorylation in EGFR tyrosine sites other than 1173 (1197) across PTPRH knockout replicates. Moreover, no significant changes in phospho-S473 AKT levels were observed in the knockouts; however, our GSEA analysis suggests downregulation of this pathway when PTPRH levels are increased. In our previous published results, we demonstrated that MMTV-*PyMT* mice harboring the conserved mutation V483M in the *Ptprh* gene present high pEGFR 1173 (1197) levels and consequent activation of the AKT pathway[24]. Similarly, PTPRH knockout in NSCLC NCI-H23 cells significantly increases pEGFR 1173 (1197) levels with a consequent increase in growth and proliferation. Nonetheless, the phosphorylation status of S473 AKT varied across the clones[23]. These conflicting findings are possibly explained by variations in research models (mouse vs human)[46], differences in mutation types (point mutations vs frameshift)[47], and compensation mechanisms by other RPTPs[48]. As we have used PTPRH knockout cell

lines previously generated by our group, we believe that after several passages, the knockout lines quickly drifted from the original phenotype and other phosphatases started to compensate for the ablation of PTPRH activity. Our RNA-sequencing results corroborate this theory, as we have observed that the H23 PTPRH knockout cells cluster surprisingly closely to the H23 PTPRH overexpressed cells, suggesting similar transcriptome profiles. In fact, studies in mice and *Drosophila* revealed that ablation of phosphatase genes leads to mild or no change in phenotype, likely due to redundancy in tyrosine phosphatase functions[38,48,49]. Additionally, we have also observed the up and downregulation of several other PTPs when PTPRH is overexpressed. Some of them have been described as EGFR regulators, including *PTPN2*[50], *PTPN6* (SHP-1)[51,52], *PTPN11* (SHP-2)[53], *PTPN12*[54], *PTPRK*[55,56], and *PTPRJ*[57,58]. Interestingly, PTPRJ dephosphorylates EGFR at the same tyrosine residue as PTPRH in a pH-dependent manner[57]. As PTPRJ is strongly downregulated in our PTPRH overexpressed cell lines, we believe that these two phosphatases have redundant roles.

In addition to our group, EGFR regulation by PTPRH has been reported by Yao and collaborators[25] and Nishiyama *et al*[59]. EGFR was first identified as a novel PTPRH interactor through a wide mammalian-membrane two-hybrid assay using 48 cloned mammalian receptor tyrosine kinases and 108 protein tyrosine phosphatases[25]. This interaction was further validated by PTPRH and EGFR co-immunoprecipitation in HEK293 cells, suggesting that, in embryonic kidney cells, the interaction between the two proteins is stable. Furthermore, in the HER2-positive breast cancer cell line SKBR-3, PTPRH was shown to be only partly involved in EGFR dephosphorylation, raising the hypothesis that more than one phosphatase is in charge of controlling inactivation of the EGFR pathway[59]. PTPRH sequestering by the connector enhancer of kinase suppressor of Ras1 (CNKSR1) prevents EGFR dephosphorylation in the SKBR-3 cells and the association between these two proteins was shown to be mediated by the intracellular phosphatase domain. Considering the mechanistic differences in the various cell lines, we cannot rule out the possibility that PTPRH interacts with different proteins depending on the cellular context. This is particularly true in this case, as we did not see a stable or transient interaction between PTPRH and EGFR in any of the three NSCLC cell lines tested herein. Of note, the labeling radius of the BioID2 molecule is ~10 nm[42]; thus if EGFR is slightly outside our PTPRH-BioID2 construct range, no signal will be detected. This finding in combination with our observation that deletion of PTPRH's phosphatase domain decreases pEGFR 1173 (1197) levels at comparable levels as wild-type PTPRH overexpression leads us to hypothesize that PTPRH acts in an intermediate pathway rather than being the primary responsible for EGFR dephosphorylation. This is the case of PTPRO, for example, which negatively regulates EGFR through direct interaction with SRC[60]. Since we observed a strong interaction between PTPRH and NFKB2 in our BioID results and NF-κB is activated downstream of the EGFR pathway through the IKK complex[61,62], this raises the possibility that PTPRH negatively regulates EGFR

through NFKB2. This agrees with the finding that there is a crosstalk between NF-κB and EGFR signaling and that transcription of NF-κB target genes influences activation of EGFR-dependent pathways[63]. Importantly, gene expression of EGFR and EGFR-related pathways were also downregulated significantly in our RNA-seq results, suggesting that PTPRH also negatively regulates EGFR at the RNA level. Further studies are needed to clarify where in time and space PTPRH fits into the proposed mechanism.

To shed light on protein regulation by PTPRH and its interaction partners, we built a comprehensive protein-protein interaction network based on stable and transient interactions revealed by BioID. We found that the top 3 candidate interactors are PTPRH itself, followed by HELZ2, and RCF2. PTPRH and other receptor protein tyrosine phosphatases form homodimers and it is speculated that this is a mechanism of inactivation of the phosphatase activity[34,43]. Hence, PTPRH dimers may be present in our cell lines or PTPRH monomers are biotinylating themselves. Even though some of the interacting proteins herein reported are mostly found in the nucleus, there is also evidence of the location of these proteins in the cytosol or the mebrane[64–66]. Since we did not observe the presence of the phosphatase in the nucleus of our transduced cells but rather in the cytosol and plasma membrane, we anticipate that the interaction is mediated in these cellular compartments. However, the Human Protein Atlas reports the presence of PTPRH nuclear speckles, hence, we cannot rule out PTPRH trafficking to the nucleus[67].

Functional and pathway enrichment analysis of interacting proteins and DEG demonstrated for the first time that PTPRH participates in novel cellular and biological processes in NSCLC cell lines. Pathways linked to RNA (binding, processing, and splicing) and ribosomal proteins (translation and biogenesis) were enriched at both the protein and RNA levels. In addition, GSEA analysis revealed the downregulation of several oncogenic signatures and hallmark pathways in NSCLC cells overexpressing PTPRH, establishing a link for how this phosphatase may contribute to lung cancer progression. These include NFE2L2, KRAS-associated pathways (MEK, RAF), LEF1, p53, BMI1, ERBB2, IL6-JAK-STAT3 signaling axis, interferon response, IL-21, reactive oxygen species, estrogen response, and metabolism of fatty acids. Curiously, these cells show upregulation of DNA repair and chromatin remodeling pathways, Wnt signaling, besides processes linked to cellular proliferation, such as E2F1 targets, G2M checkpoint, and chromosome organization. A few studies were published in the early 2000s implying that PTPRH participates in some other cellular processes. Overexpression of the phosphatase in Chinese hamster ovary cells disrupted cellular responses mediated by integrins (cell growth and motility) by dephosphorylation of focal adhesion-associated proteins[31]. In Jukart T cells, PTPRH inhibits the T cell antigen receptor (TCR) activity by interacting with the kinase Lck[29]. Moreover, overexpression of PTPRH in NIH 3T3 fibroblasts was shown to induce apoptosis mediated by the inactivation of the PI3K-AKT-ILK pathway

and activation of cell death pathways dependent on caspases[33]. Even though in our study we did not observe PTPRH participation in integrins or caspases-mediated pathways, our pathway enrichment analysis revealed the downregulation of several pathways controlling proliferation, AKT, and some immune-related pathways as mentioned above. All these findings highlight differences in functionality according to the cell type and condition.

When tyrosine kinases were analyzed separately, we found that gene expression of several of them is modulated upon overexpression of PTPRH in a significant manner. There is strong upregulation of FLT3, EPHB1, KIT, ROR2, NTRK1, PDGFRA, EPHB6, and EPHA7, and downregulation of MST1R, EPHA8, ERBB3, LMTK3, TEK, ROR1, FGFR1, and PDGFRB, besides EGFR. This could also be a consequence of the variety of PTPs that are perturbed concomitantly. In addition, we had previously reported that the phosphorylated levels of FGFR1 increase upon ablation of PTPRH in H23 cells[23].

In summary, we found that PTPRH indirectly regulates the EGFR pathway at both the RNA and protein levels and is primarily involved in RNA and translation-associated pathways in NSCLC cells. Moreover, overexpression of the phosphatase negatively modulated several oncogenic signature pathways and genes, shedding light on how this phosphatase may contribute to lung cancer progression.

Methods

Cell culture

Cells were acquired from ATCC and H23 PTPRH knockout cells were generated as described previously[23]. NCI-H23 cells and derived lineages were cultured in RPMI medium (Corning #50-020-PC) supplemented with 10% fetal bovine serum, 1% Penicillin-Streptomycin, 23.8 mM sodium bicarbonate, 25 mM HEPES, and 1 mM sodium pyruvate. NCI-H2023 and derived lineages were cultured in DMEM-F12/HEPES medium (Gibco #11330032) supplemented with 5% fetal bovine serum (FBS), 1% Penicillin-Streptomycin, 30nM sodium selenite, 10 nM hydrocortisone, 10 nM beta-estradiol, 0.01 mg/mL transferrin, 0.005 mg/mL insulin, and 2 mM L-glutamine. HT-29 cells were cultured in McCoy's 5a (modified) medium (Gibco #16600082) supplemented with 10% FBS and 1% Penicillin-Streptomycin. 293T cells were cultured in DMEM high glucose medium (Sigma-Aldrich #56436C) supplemented with 10% FBS and 1% Penicillin-Streptomycin. Cells were incubated at 37°C and 5% CO_2 and split using 0.25% Trypsin (Gibco #15090046) when 80% confluency was reached.

EGF stimulation

Recombinant human EGF (Gibco #PHG0311) was added to the medium of NCI-H23 or H23 KO cells at 80% confluency to reach a final concentration of 100 ng/mL. Cells were incubated at 37°C and 5% CO_2 for 2, 5, 10, 15, 30, 60, or 120 minutes. Cells were washed twice with ice-cold HEPES- Buffered Saline (HBS) to stop stimulation followed by cell lysis to collect proteins.

Cell lysis and protein collection

After washing twice with ice-cold HBS, cells were scrapped from the dish and resuspended in ice-cold HBS. The cell suspension was centrifuged at 1,000 x g for 5 minutes at 4°C, followed by lysis in ice with ice-cold Pierce RIPA buffer (immunoblot and LC/MS/MS experiments) (Thermo Scientific #89901) or IP lysis/wash buffer (co-immunoprecipitation experiments) (Pierce Classic Magnetic IP/Co-IP kit #88804) +

Halt Protease and Phosphatase inhibitor (Thermo Scientific #78441) for 20 minutes. Cell extracts were centrifuged at 16,000 x g for 20 minutes at 4°C and the supernatant containing the protein fraction was collected and stored at -80°C until use. Protein quantification was performed using Pierce BCA protein assay (Thermo Scientific #23225) according to the manufacturer's instructions.

Immunoblotting and Densitometry

Protein samples were prepared using Laemmli SDS reducing sample buffer (Thermo Scientific #J61337-AC), followed by boiling in the dry bath at 95°C for 10 minutes. Samples were loaded in an 8% SDS-PAGE gel and electrophoresis was conducted at 100 V in Tris/Glycine/SDS buffer (BioRad #1610732). Following, samples were transferred to a PVDF Immobilon-P membrane (Millipore #IPVH00010) at 100 V for 1,5 hours at 4°C in ice-cold Tris/Glycine buffer containing 20% methanol. Membranes were blocked in 5% non-fat dry milk (diluted in TBS-Tween 0.1%) for one hour at room temperature (RT) under agitation and washed 3 times for 5 minutes with TBS-Tween 0.1% in the shaker. Primary antibodies were diluted in TBS-Tween 0.1% and 5% bovine serum albumin (BSA) and incubated with the membrane overnight at 4°C under agitation. The following dilutions were used for the primary antibodies: PTPRH 1:1000 (Abcam #ab231767), pEGFR 1173 1:500 (Cell Signaling #4407), EGFR 1:1000 (Cell Signaling #4267), B-actin 1:1000 (Cell Signaling #4967), HA Tag 1:1000 (Cell Signaling #3724), anti-Biotin 1:1000 (Cell Signaling #5597), BioID2 1:20000 (BioFront Technologies #BID2-CP-100), pAKT S473 1:2000 (Cell Signaling #4060), AKT 1:1000 (Cell Signaling #4685), and Vinculin 1:1000 (Cell Signaling #13901). Following 3 washes of 5 minutes with TBS-Tween 0.1% at RT, membranes were incubated for one hour and under agitation with fluorescent IRDye® 800CW goat anti-rabbit (LICOR #926-32211) or donkey anti-chicken (LICOR #926-32218) secondary antibodies diluted 1:10000 in TBS-Tween 0.1% and 5% BSA. Unbound antibodies were removed by washing the membranes three times, 5 minutes/each, with TBS-Tween 0.1%. Images were taken using the LICOR Odyssey M machine.

Densitometry was performed using ImageJ 1.54d software. First, the area selection size was set based on the sample with the largest band for each target protein (e.g. pEGFR 1173 and EGFR) and the loading control (i.e. B-actin). The grey mean value (X) of the band and background values for all samples were then measured and recorded. After the measurements were inverted using the 255-X formula, the background of each sample was subtracted from their band values. The resulting values for the target proteins were then divided by B-actin for data normalization. Finally, the normalized phospho-protein values were divided by the normalized total protein values of each sample to obtain the phospho-photein/total protein ratios.

Immunoprecipitation and Co-immunoprecipitation

Protein lysates containing the same amount of protein from EGF-stimulated cells were mixed with EGFR monoclonal antibody (Cell Signaling #4267, 1:50 dilution) and incubated overnight at 4°C using end-to-end rotation. 50 mg of Dynabeads Protein A (Thermo Scientific #10006D) was added to the antibody-antigen conjugate and incubated at RT for 30 min using rotation. Samples were placed in a magnetic rack and the supernatant was discarded. The magnetic bead-antibody-antigen complex was washed and eluted as recommended by the manufacturer. The immunoprecipitated fraction was then analyzed for co-immunoprecipitation of EGFR and PTPRH by immunoblotting as described previously or sent to LC/MS/MS for screening of phospho-tyrosine sites.

Mass Spectrometry

LC/MS/MS was performed at the MSU Mass Spectrometry Core. On-bead antibody-bound proteins were first washed 3 times with 50 mM ammonium bicarbonate and digested with trypsin (5 ng/uL, incubation at 37°C for 6 hours). The solution was acidified using 1% trifluoroacetic acid and centrifuged at 14000 x g. After supernatant collection, the peptides were concentrated by solid phase extraction using StageTips[68] and dried by vacuum centrifugation. An injection of 10 uL of dried peptides resuspended in 2% acetonitrile and 0.1% trifluoroacetic acid was conducted using the Thermo Scientific EASY-nLC 1200 system and 0.1mm x 20 mm Acclaim™ PepMap™ C18 RSLC trapping columns (Thermo Scientific), followed by a 5min wash with buffer A (99.9% Water/0.1% Formic Acid). Peptides were eluted for 35 minutes onto a 0.075 mm x 500 mm Acclaim™ PepMap™ RSLC resolving column (Thermo Scientific) using a liner gradient ranging from 5-28% of buffer B (80% Acetonitrile/0.1% Formic Acid/19.9% Water) for 24 minutes. Next, column wash was performed using 90% buffer B for 10 minutes (constant flow rate = 300nl/min). Column temperature was kept constant at 50°C with the aid of an integrated column oven-PRSO-V2 (Sonation GmbH). Using a FlexSpray ion source, the peptides were then sprayed into the Q-Exactive mass spectrometer (Thermo Scientific) and survey scans of 45000 resolution (based on m/z 200) were collected using Orbi trap. The predominant 15 ions from each survey underwent an automatic higher energy collision-induced association (HCD) and the resulting fragment spectra were collected using a resolution of 7500. These spectra were then transformed into a peaks list by the software Mascot Distiller v2.8.3. Using the Mascot[2] searching algorithm v 2.8.0.1, the peaks list was compared to a human protein database containing all sequences from UniProt and supplemented with frequent laboratory contaminants (downloaded from www.thegpm.org, cRAP project). Parameters were set to allow up to 2 missed tryptic sites, fixed modification of carbamidomethyl cysteine, variable modification of oxidation of Methionine and/or phosphorylation of Tyrosine, MS/MS tolerance of 0.02 Da, and peptide tolerance +/- 10 ppm. Following, the output list was analyzed using Scaffold v5.3.0. Proteins identified with 99% protein threshold, 95% peptide threshold, and 2 minimum peptide number were considered true. Quantitative

analysis was performed based on normalized total precursor intensity and missing values were replaced by imputation (1,000 or 10,000).

Plasmids

pCMV-VSV-G was a gift from Bob Weinberg (Addgene plasmid # 8454), pCMV delta R8.2 was a gift from Didier Trono (Addgene plasmid # 12263), and MCS-BioID2-HA pBabe-puro was a gift from Kyle Roux (Addgene plasmid #120308). The lentiviral PTPRH WT- HA plasmid was prebuilt by Addgene. Briefly, the lentiCas9-Blast plasmid (Addgene plasmid # 52962), a gift from Feng Zhang, was modified to replace the Cas9 sequence with the human *PTPRH* coding sequence (CCDS 33110.1) and a C-terminal HA tag. A map of the generated plasmid is provided in the supplementary figure 1C.

Bacterial Transformation and Plasmid Prep

DH5-α competent cells were transformed by heat shock. 100 uL of ice-thawed cells were added to a centrifuge tube containing ~5 ng of purified plasmid. The mixture was incubated for 30 minutes in ice, followed by 45 seconds in the 42°C water bath, and 2 minutes in ice. 500 uL of warm SOC outgrowth medium (New England Biolabs #B9020S) was added to the tubes and the mixture was incubated overnight at 37°C and 220 rpm agitation. On the next day, transformed bacteria were streaked onto LB agar plates containing ampicillin (100 ug/mL) and incubated at 37°C overnight. Following, single-grown colonies were diluted in warm LB broth + ampicillin (100 ug/mL) and incubated at 37°C and 220 rpm agitation overnight. Plasmids were recovered using Monarch Plasmid Miniprep Kit (New England Biolabs #T1010S) or E.Z.N.A. Plasmid DNA Midi Kit (Omega Bio-tek #D6904). Full-length sequencing was carried out by Plasmidsaurus using Oxford Nanopore Technologies.

Site-Directed Mutagenesis

To generate PTPRH constructs with deletions in various sites, primers were designed using the NEBaseChanger software (https://nebasechanger.neb.com/) using the human *PTPRH* coding sequence (CCDS 33110.1) as a template. The sequence of the primers is described in the table below. Mutagenesis was carried out in the PTPRH WT- HA plasmid using the Q5 Site-Direct Mutagenesis Kit (New England Biolabs #E0554) according to the manufacturer's instructions. The generated plasmids were sequenced as previously described and sequencing results were aligned against the human *PTPRH* coding sequence using local pairwise alignment (MAFFT v7) from Benchling. Constructs containing *in-frame* deletions in the intended site were used for lentiviruses generation and cell transduction.

Construct	Forward (5` - 3`)	Reverse (5` - 3`)

Δ1	ACTCGAAATGCCACCACAGCTCACAACCCAG	GGGGGCAGGCGCCCTGGC
Δ2	TCCGTGTGGGTGGGGAAG	GTTGTGAGCTGTGGTGGC
Δ3	ACCCTCACTGCAGCCACT	AGTCTCCATATGGAGGTTTCTCAC
Δ4	CAACAGTCAGCCCAGGCC	GTGGAATTGGCGCACAGAC

Lentivirus Generation and Cell Transduction

293T cells were seeded on 10 cm dishes (3 x 10^6 cells/dish) on the day before the transfection. On the next day, pCMV-VSV-G, pCMV delta R8.2, and transfer plasmid were mixed with PEI Prime (Sigma-Aldrich #919012) in Opti-MEM medium (Gibco #11058021) in a 1 DNA: 3 PEI ratio and added to the cells. Mock viruses were generated using pCMV-VSV-G and pCMV delta R8.2 only. After 6 hours of incubation, the medium was discarded, and cells were replenished with a complete DMEM high glucose medium. The supernatant containing the lentiviruses was harvested at 48 and 72 hours after transfection and filtered through a 0.45 µm Millex PES filter (Millipore Sigma #SLHPR33RS). The lentiviruses were concentrated 10x using Lenti-X Concentrator (Takara Bio #631232) following the manufacturer's instructions and stored at -80°C.

For the transduction step, target cells were plated in 6-well plates using 10^5 cells/well on day 1. On the next day, when cells were ~40% confluent, a mixture of complete media, Viral Entry Transduction Enhancer (abm #G515), and an equal volume of lentiviruses were added. The transduction was stopped on day 3 by replenishing the cells with a fresh complete medium. On day 5, we started the selection of infected cells with blasticidin (Dot Scientific Inc. #3513-03-9). We defined the optimal antibiotic concentration using a killing curve, and NCI-H2023 and NCI-H23 (parental and transduced) were treated with 4, 6, and 8 ug/mL of blasticidin, respectively. The selection was stopped when all parental cells were dead.

BioID2 experiment

BioID2-HA was cloned downstream of the EF-1α core promoter into the C-terminal of *PTPRH* WT or an empty lentiviral backbone to generate the PTPRH WT-BioID2 or BioID2-only plasmids, respectively, using the golden gate method. To generate the PTPRH WT linearized vector, the PTPRH-HA WT plasmid was amplified to include all sequences but the HA tag using the primers F: 5' GACCTCCAACTTGTGGGC 3' and R: 5' GGATCCGGCGCAACAAAC 3'. To generate a linearized empty lentiviral backbone (without the PTPRH WT-HA sequence), the same plasmid was amplified using

the primers F: 5' ACCGGTCCTGTGTTCTGG 3' and R: 5' GGATCCGGCGCAACAAAC3'. BioID2-HA sequence was extracted from MCS-BioID2-HA pBabe-puro using the primers F: 5' aagtttgttgcgccggatccTGCGTAATCCGGTACATC 3' and R: 5' aggcccacaagttggaggtcTTCAAGAACCTGATCTGG 3' or F: 5' aagtttgttgcgccggatccTGCGTAATCCGGTACATC 3' and R: 5' cgccagaacacaggaccggtgccaccatgTTCAAGAACCTGATCTGG 3' to include the start codon ATG. The lower caps letters in the primer sequences indicate the overlapping regions with the vector. Platinum Superfi II PCR MM (Invitrogen #12368010) was used for all amplification reactions following the manufacturer's instructions. The PCR products were purified using the Monarch DNA and PCR Cleaning kit (New England Biolabs #T1030S) and templates were digested using Dnp1 (New England Biolabs #R0176). Assembly reaction was performed at 1:2 vector: insert ratio using the NEBuilder HiFi DNA Assembly Cloning Kit (New England Biolabs #E5520) according to the manufacturer's protocol. After bacterial transformation and purification of the generated plasmid, lentiviruses were produced as previously described.

NCI-H2023 and H23 KO cells were transduced with BioID2-only, PTPRH WT-BioID2, or mock lentiviruses. Cells expressing the BioID2-only and PTPRH WT-BioID2 transgenes were selected by treatment with blasticidin and all cell lines were expanded to 100 mm cell culture dishes (n= 3 technical replicates/cell line). When ~ 60% confluency was reached, cells were serum-starved for 24 hours by adding fresh complete medium without FBS. After the incubation period, the old medium was removed, and cells were replenished with a complete medium containing FBS and 50 uM biotin (Thermo Scientific #29129). Cells were lysed 18 hours after treatment for protein collection and analyzed by immunoblotting. For immunoprecipitation of biotinylated proteins, 800 ug of protein lysates and 0.5 mg of MagReSyn Streptavidin MS beads (ReSyn Bio #MR-STV002) equilibrated in Pierce RIPA buffer + Halt Protease and Phosphatase inhibitor (Thermo Scientific #78441) were incubated for 24 hours at 4°C using end-to-end rotation. The washing of the antigen-bead complex was performed following the manufacturer's instructions. Next, the immunoprecipitated fraction was run in LC/MS/MS for protein identification. The analysis of PTPRH interactors adhered to the recommendations outlined by Roux *et al* [69,70]. Briefly, the identified proteins underwent initial filtration to exclude those commonly observed in biotinylation experiments, referencing the CRAPome database. Those with a CRAPome score > 300 were considered contaminants and removed from the analysis. Furthermore, histones, endogenous carboxylases, and other known BioID2 interactors (i.e. AHNAK, FLNA, PARP1, EEF1A1, PRKDC, TOP1, PKM) were manually curated. Candidate interactors were defined as having a minimum of a 3-fold increase in normalized total precursor intensity in the PTPRH WT-BioID2 group when compared to

BioID2-only and present in both of the cell lines herein tested. STRING analysis of these candidate interactors was done using Cytoscape 3.10.2.

Immunofluorescence

Mock, BioID2-only, and PTPRH WT-BioID2 cells were seeded in duplicate at 10^5 cells/well in 6-well plates containing coverslips on the day before. Cells were fixed in 4% Paraformaldehyde (PFA, pH 7.4) for 10 minutes at RT and rinsed with ice-cold PBS three times. Next, cells were permeabilized using PBS-Tween 0.4%, washed three times with PBS for 5 min/wash, and blocked with Image-iT FX signal enhancer (Invitrogen #I36933) for 30 minutes. The coverslips were then incubated with primary antibodies against BioID2 (1:5000, BioFront #BID2-CP-100) or HA tag (1:800, Cell Signaling #3724) diluted in 1% BSA/ PBS-Tween 0.1% for one hour in a humidified chamber at RT. Following three washes with PBS of 5 minutes/each, Alexa Fluor 488 goat anti-chicken (1:400, Invitrogen #A-11039) or Alexa Fluor 594 goat anti-rabbit (1:400, Invitrogen #A-11012) diluted in 1% BSA/ PBS-Tween 0.1% was added to the coverslips and incubated for 1 hour at RT. Coverslips were mounted to glass slides with Prolong Gold Antifade Mountant with DAPI (Invitrogen #P36935). Images were acquired in the Nikkon Ti2 microscope using FITC (700 ms exposure), TRITC (500 ms exposure), and DAPI (autoexposure) filters. Images were processed with ImageJ 1.54g.

qPCR

NCI-H23, A427, and HT-29 cells were seeded as triplicates in 6-well plates (2 x 10^5 cells/well) in complete medium. On the following morning, EGF was added to each well (500 ng/mL) and cells were incubated for 18 hours. Total RNA was extracted using the RNeasy Mini Kit (Qiagen #74104) according to the manufacturer's instructions. cDNA generation and qPCR were performed in one-step using 100 ng of template, 100 nM of primers (PTPRH, F: 5' TGTGCGTCCACATACCCAGA 3', R: 5' CAGCCTCCCCACATGAAGAT 3'; GAPDH, F: 5' TCATGACCACAGTGGATGCC 3', R: 5' GGAGTTGCTGTTGAAGTCGC 3'), and Power SYBR™ Green RNA-to-CT™ 1-Step Kit (Applied Biosystems #4391178) following manufacturer's protocol. ΔΔ Ct analysis was performed as described by Livak & Schmittgen.[71]

RNA-sequencing

NCI-H2023 and H23 KO cells were transduced with *PTPRH* WT-HA lentivirus to stably overexpress PTPRH and protein levels were validated by western blotting as described above. The parental and transduced cell lines were seeded as triplicates in 6-well plates (10^5 cells/well) and incubated overnight. On the next day, cells were replenished with serum-free complete medium. After 24 hours of serum

starvation, a complete medium containing FBS was added to the cells and incubated for an additional 16 hours. Total RNA was collected from the FBS-stimulated cells using RNeasy Mini Kit (Qiagen #74104) according to the manufacturer's protocol. Library preparation and paired-end RNA sequencing (Illumina PE150) were conducted by Novogene using NovaSeq X Plus Series (Illumina) using a minimum coverage of 30M reads per sample. The quality of the raw reads was assessed through *FastQC* 0.11.7 and trimmed using *Trimmomatic* 0.39. Trimmed reads were aligned against the human genome (grch38) using *Hisat2* 2.1.0 and a count matrix of raw reads to be used as input for DESeq2 was generated by *StringTie* 2.1.3 as described in the *StringTie StringTie* documentation. Differential expression analysis was performed using DESeq2 1.42.1 and differentially expressed genes (DEG) with padj < 0.05 were considered significant. The *gage* package 2.52.0 was used for gene set enrichment for pathway analysis of GO biological processes in our list of DEG, as well as GSEA for hallmark and C6 oncogenic signature gene sets from MSigDB using the *fgsea* package 1.28.0. Pathways with padj < 0.05 were considered enriched and reported in our analysis.

Data Visualization and Statistical Analysis

Data visualization and statistical tests (i.e. two-tail t-test, ANOVA) were performed in R version 4.3.3. * p < 0.05 was considered as a significant result.

References

1. Vitrac, H., Mallampalli, V. K. P. S. & Dowhan, W. Importance of phosphorylation/dephosphorylation cycles on lipid-dependent modulation of membrane protein topology by posttranslational phosphorylation. *J Biol Chem* **294**, 18853–18862 (2019).
2. Bononi, A. *et al.* Protein Kinases and Phosphatases in the Control of Cell Fate. *Enzyme Res* **2011**, 329098 (2011).
3. Qi, X.-M., Wang, F., Mortensen, M., Wertz, R. & Chen, G. Targeting an oncogenic kinase/phosphatase signaling network for cancer therapy. *Acta Pharmaceutica Sinica B* **8**, 511–517 (2018).
4. Ardito, F., Giuliani, M., Perrone, D., Troiano, G. & Lo Muzio, L. The crucial role of protein phosphorylation in cell signaling and its use as targeted therapy (Review). *International Journal of Molecular Medicine* **40**, 271–280 (2017).
5. Turdo, A. *et al.* Targeting Phosphatases and Kinases: How to Checkmate Cancer. *Front Cell Dev Biol* **9**, 690306 (2021).
6. Harrison, P. T., Vyse, S. & Huang, P. H. Rare epidermal growth factor receptor (EGFR) mutations in non-small cell lung cancer. *Seminars in Cancer Biology* **61**, 167–179 (2020).
7. Gijtenbeek, R. G. P. *et al.* Overall survival in advanced epidermal growth factor receptor mutated non-small cell lung cancer using different tyrosine kinase inhibitors in The Netherlands: a retrospective, nationwide registry study. *The Lancet Regional Health – Europe* **27**, (2023).
8. Amrhein, J. A. *et al.* Macrocyclization of Quinazoline-Based EGFR Inhibitors Leads to Exclusive Mutant Selectivity for EGFR L858R and Del19. *J. Med. Chem.* **65**, 15679–15697 (2022).
9. Reguart, N. & Remon, J. Common EGFR-mutated subgroups (Del19/L858R) in advanced non-small-cell lung cancer: chasing better outcomes with tyrosine kinase inhibitors. *Future Oncol* **11**, 1245–1257 (2015).
10. Galdadas, I. *et al.* Structural basis of the effect of activating mutations on the EGF receptor. *eLife* **10**, e65824.

11. Red Brewer, M. *et al.* Mechanism for activation of mutated epidermal growth factor receptors in lung cancer. *Proceedings of the National Academy of Sciences* **110**, E3595–E3604 (2013).

12. Gazdar, A. Activating and resistance mutations of EGFR in non-small-cell lung cancer: role in clinical response to EGFR tyrosine kinase inhibitors. *Oncogene* **28**, S24–S31 (2009).

13. Liu, Q. *et al.* EGFR-TKIs resistance via EGFR-independent signaling pathways. *Molecular Cancer* **17**, 53 (2018).

14. Hsu, P.-C., Jablons, D. M., Yang, C.-T. & You, L. Epidermal Growth Factor Receptor (EGFR) Pathway, Yes-Associated Protein (YAP) and the Regulation of Programmed Death-Ligand 1 (PD-L1) in Non-Small Cell Lung Cancer (NSCLC). *Int J Mol Sci* **20**, 3821 (2019).

15. Grosse, A., Grosse, C., Rechsteiner, M. & Soltermann, A. Analysis of the frequency of oncogenic driver mutations and correlation with clinicopathological characteristics in patients with lung adenocarcinoma from Northeastern Switzerland. *Diagnostic Pathology* **14**, 18 (2019).

16. Dang, A.-T. H. *et al.* Actionable Mutation Profiles of Non-Small Cell Lung Cancer patients from Vietnamese population. *Sci Rep* **10**, 2707 (2020).

17. cBioPortal for Cancer Genomics. https://www.cbioportal.org/.

18. Du, Z. & Lovly, C. M. Mechanisms of receptor tyrosine kinase activation in cancer. *Mol Cancer* **17**, 58 (2018).

19. Bollu, L. R., Mazumdar, A., Savage, M. I. & Brown, P. H. Molecular Pathways: Targeting Protein Tyrosine Phosphatases in Cancer. *Clinical Cancer Research* **23**, 2136–2142 (2017).

20. Gkountakos, A. *et al.* PTEN in Lung Cancer: Dealing with the Problem, Building on New Knowledge and Turning the Game Around. *Cancers (Basel)* **11**, 1141 (2019).

21. Sirhan, Z., Alojair, R., Thyagarajan, A. & Sahu, R. P. Therapeutic Implications of PTEN in Non-Small Cell Lung Cancer. *Pharmaceutics* **15**, 2090 (2023).

22. Richards, C. E. *et al.* Protein Tyrosine Phosphatase Non-Receptor 11 (PTPN11/Shp2) as a Driver Oncogene and a Novel Therapeutic Target in Non-Small Cell Lung Cancer (NSCLC). *Int J Mol Sci* **24**, 10545 (2023).

23. Swiatnicki, M. R. *et al.* Elevated phosphorylation of EGFR in NSCLC due to mutations in PTPRH. *PLOS Genetics* **18**, e1010362 (2022).

24. Rennhack, J. P. *et al.* Integrated analyses of murine breast cancer models reveal critical parallels with human disease. *Nat Commun* **10**, 3261 (2019).

25. Yao, Z. *et al.* A Global Analysis of the Receptor Tyrosine Kinase-Protein Phosphatase Interactome. *Mol Cell* **65**, 347–360 (2017).

26. Protein tyrosine phosphatases: from genes, to function, to disease | Nature Reviews Molecular Cell Biology. https://www.nature.com/articles/nrm2039.

27. Matozaki, T. *et al.* Molecular cloning of a human transmembrane-type protein tyrosine phosphatase and its expression in gastrointestinal cancers. *J Biol Chem* **269**, 2075–2081 (1994).

28. Phosphotyrosine phosphatase R3 receptors: Origin, evolution and structural diversification | PLOS ONE. https://journals.plos.org/plosone/article?id=10.1371/journal.pone.0172887.

29. Interaction of SAP-1, a Transmembrane-type Protein-tyrosine Phosphatase, with the Tyrosine Kinase Lck: ROLES IN REGULATION OF T CELL FUNCTION - ScienceDirect. https://www.sciencedirect.com/science/article/pii/S0021925820835364?via%3Dihub.

30. Protein tyrosine phosphatase SAP-1 protects against colitis through regulation of CEACAM20 in the intestinal epithelium | PNAS. https://www.pnas.org/doi/full/10.1073/pnas.1510167112.

31. Inhibition of Cell Growth and Spreading by Stomach Cancer-associated Protein-tyrosine Phosphatase-1 (SAP-1) through Dephosphorylation of p130cas - ScienceDirect. https://www.sciencedirect.com/science/article/pii/S0021925819568181?via%3Dihub.

32. Nishiyama, K. *et al.* CNKSR1 serves as a scaffold to activate an EGFR phosphatase via exclusive interaction with RhoB-GTP. *Life Science Alliance* **4**, (2021).

33. Induction of Apoptosis by Stomach Cancer-associated Protein-tyrosine Phosphatase-1 - ScienceDirect. https://www.sciencedirect.com/science/article/pii/S002192582074336X?via%3Dihub.

34. Wälchli, S., Espanel, X. & Hooft van Huijsduijnen, R. Sap-1/PTPRH activity is regulated by reversible dimerization. *Biochem Biophys Res Commun* **331**, 497–502 (2005).

35. Seo, Y. *et al.* Overexpression of SAP-1, a Transmembrane-Type Protein Tyrosine Phosphatase, in Human Colorectal Cancers. *Biochemical and Biophysical Research Communications* **231**, 705–711 (1997).

36. Chen, A., Ding, S., Shen, X. & Lin, X. The High Expression of PTPRH Is Associated with Poor Prognosis of Human Lung Adenocarcinoma. *Computational and Mathematical Methods in Medicine* **2021**, e9932088 (2021).

37. Bujko, M. *et al.* Downregulation of PTPRH (Sap-1) in colorectal tumors. *International Journal of Oncology* **51**, 841–850 (2017).

38. Sadakata, H. *et al.* SAP-1 is a microvillus-specific protein tyrosine phosphatase that modulates intestinal tumorigenesis. *Genes to Cells* **14**, 295–308 (2009).

39. Nagano, H. *et al.* Downregulation of stomach cancer-associated protein tyrosine phosphatase-1 (SAP-1) in advanced human hepatocellular carcinoma. *Oncogene* **22**, 4656–4663 (2003).

40. Capuani, F. *et al.* Quantitative analysis reveals how EGFR activation and downregulation are coupled in normal but not in cancer cells. *Nat Commun* **6**, 7999 (2015).

41. Salazar-Cavazos, E. *et al.* Multisite EGFR phosphorylation is regulated by adaptor protein abundances and dimer lifetimes. *MBoC* **31**, 695–708 (2020).

42. Kim, D. I. *et al.* An improved smaller biotin ligase for BioID proximity labeling. *MBoC* **27**, 1188–1196 (2016).

43. Tonks, N. K. Protein tyrosine phosphatases: from genes, to function, to disease. *Nat Rev Mol Cell Biol* **7**, 833–846 (2006).

44. Schroder, W. A. *et al.* SerpinB2 inhibits migration and promotes a resolution phase signature in large peritoneal macrophages. *Sci Rep* **9**, 12421 (2019).

45. Moidu, N. A., A Rahman, N. S., Syafruddin, S. E., Low, T. Y. & Mohtar, M. A. Secretion of pro-oncogenic AGR2 protein in cancer. *Heliyon* **6**, e05000 (2020).

46. Ortiz, M. M. O. & Andrechek, E. R. Molecular Characterization and Landscape of Breast cancer Models from a multi-omics Perspective. *J Mammary Gland Biol Neoplasia* **28**, 12 (2023).

47. Genetic Mutation | Learn Science at Scitable. http://www.nature.com/scitable/topicpage/genetic-mutation-1127.

48. Sun, Q., Schindelholz, B., Knirr, M., Schmid, A. & Zinn, K. Complex genetic interactions among four receptor tyrosine phosphatases regulate axon guidance in Drosophila. *Mol Cell Neurosci* **17**, 274–291 (2001).

49. den Hertog, J. & van Eekelen, M. Chapter 101 - Zebrafish and Phosphatase Function. in *Handbook of Cell Signaling (Second Edition)* (eds. Bradshaw, R. A. & Dennis, E. A.) 827–833 (Academic Press, San Diego, 2010). doi:10.1016/B978-0-12-374145-5.00101-7.

50. Stanoev, A. *et al.* Interdependence between EGFR and Phosphatases Spatially Established by Vesicular Dynamics Generates a Growth Factor Sensing and Responding Network. *Cell Syst* **7**, 295-309.e11 (2018).

51. Wu, Y. *et al.* Protein tyrosine phosphatase SHP-1 sensitizes EGFR/HER-2 positive breast cancer cells to trastuzumab through modulating phosphorylation of EGFR and HER-2. *OTT* **8**, 2577–2587 (2015).

52. Forbes, K., Skinner, L., Aplin, J. D. & Westwood, M. The tyrosine phosphatase SHP-1 negatively regulates cytotrophoblast proliferation in first-trimester human placenta by modulating EGFR activation. *Cell. Mol. Life Sci.* **69**, 4029–4040 (2012).

53. Agazie, Y. M. & Hayman, M. J. Molecular Mechanism for a Role of SHP2 in Epidermal Growth Factor Receptor Signaling. *Mol Cell Biol* **23**, 7875–7886 (2003).

54. Sun, T. *et al.* Activation of multiple proto-oncogenic tyrosine kinases in breast cancer via loss of the PTPN12 phosphatase. *Cell* **144**, 703–718 (2011).

55. Xu, Y., Tan, L.-J., Grachtchouk, V., Voorhees, J. J. & Fisher, G. J. Receptor-type Protein-tyrosine Phosphatase-κ Regulates Epidermal Growth Factor Receptor Function*. *Journal of Biological Chemistry* **280**, 42694–42700 (2005).

56. Xu, Y. *et al.* Receptor Type Protein Tyrosine Phosphatase-Kappa Mediates Cross-Talk between Transforming Growth Factor-Beta and Epidermal Growth Factor Receptor Signaling Pathways in Human Keratinocytes. *MBoC* **21**, 29–35 (2010).

57. Rizzo, S. *et al.* Promoting the activity of a receptor tyrosine phosphatase with a novel pH-responsive transmembrane agonist inhibits cancer-associated phenotypes. *Protein Science* **32**, e4742 (2023).

58. Schwarz, M. *et al.* Disrupting PTPRJ transmembrane-mediated oligomerization counteracts oncogenic receptor tyrosine kinase FLT3 ITD. *Front. Oncol.* **12**, (2022).

59. Nishiyama, K. *et al.* CNKSR1 serves as a scaffold to activate an EGFR phosphatase via exclusive interaction with RhoB-GTP. *Life Sci Alliance* **4**, e202101095 (2021).

60. Asbagh, L. A. *et al.* The tyrosine phosphatase PTPRO sensitizes colon cancer cells to anti-EGFR therapy through activation of SRC-mediated EGFR signaling. *Oncotarget* **5**, 10070–10083 (2014).

61. Blakely, C. M. *et al.* NF-κB activating complex engaged in response to EGFR oncogene inhibition drives tumor cell survival and residual disease in lung cancer. *Cell Rep* **11**, 98–110 (2015).

62. Biswas, D. K., Cruz, A. P., Gansberger, E. & Pardee, A. B. Epidermal growth factor-induced nuclear factor κB activation: A major pathway of cell-cycle progression in estrogen-receptor negative breast cancer cells. *Proceedings of the National Academy of Sciences* **97**, 8542–8547 (2000).

63. Shostak, K. & Chariot, A. EGFR and NF-κB: partners in cancer. *Trends in Molecular Medicine* **21**, 385–393 (2015).

64. Huntzinger, E., Sinteff, J., Morlet, B. & Séraphin, B. HELZ2: a new, interferon-regulated, human 3′-5′ exoribonuclease of the RNB family is expressed from a non-canonical initiation codon. *Nucleic Acids Res* **51**, 9279–9293 (2023).

65. Fagerlund, R., Kinnunen, L., Köhler, M., Julkunen, I. & Melén, K. NF-{kappa}B is transported into the nucleus by importin {alpha}3 and importin {alpha}4. *J Biol Chem* **280**, 15942–15951 (2005).

66. The Human Protein Atlas. https://www.proteinatlas.org/.

67. PTPRH protein expression summary - The Human Protein Atlas. https://www.proteinatlas.org/ENSG00000080031-PTPRH.

68. Rappsilber, J., Mann, M. & Ishihama, Y. Protocol for micro-purification, enrichment, pre-fractionation and storage of peptides for proteomics using StageTips. *Nat Protoc* **2**, 1896–1906 (2007).

69. Roux, K. J., Kim, D. I., Burke, B. & May, D. G. BioID: A Screen for Protein-Protein Interactions. *Curr Protoc Protein Sci* **91**, 19.23.1-19.23.15 (2018).

70. Sears, R. M., May, D. G. & Roux, K. J. BioID as a Tool for Protein-Proximity Labeling in Living Cells. *Methods Mol Biol* **2012**, 299–313 (2019).

71. Livak, K. J. & Schmittgen, T. D. Analysis of relative gene expression data using real-time quantitative PCR and the 2(-Delta Delta C(T)) Method. *Methods* **25**, 402–408 (2001).

Figure Legends

Figure 1. Investigation of pEGFR 1173 (1197) levels on H23 PTPRH knockout cell lines.

H23 and H23 PTPRH KO cells were stimulated with EGF (100 ng/mL) and cell lysates collected after 5, 15, 30, 60 and 120 minutes (A). Time point 0 represents non-stimulated (untreated) cells. Differences in pEGFR 1173 (1197) (n=4/group in each time point) and pAKT S473 (n=3/group in each time point) levels were assessed by immunoblot and representative blots are shown (mean +/- s.d.). Results of densitometry for pEGFR 1173 (1197)/total EGFR and pAKT/Total AKT ratio for the replicates are demonstrated as individual dots in the bar plots. T-test was performed to compare the PTPRH KO group with the parental cell (H23) in each time point and *$p<0.05$ was considered a significant result. B) EGFR was immunoprecipitated from H23 (n=2) and H23 PTPRH KO (n=3) cells stimulated with EGF (100 ng/mL) for 15 minutes and sent for mass spectrometry analysis. Quantitative values of normalized total precursor intensities for the identified phospho-Tyr sites in each cell line are represented in the table and the bar plot (mean +/- s.d.). Abbreviations: ns = non-significant; Tyr (Y) = tyrosine; IB = immunoblot

Figure 2. Investigating pEGFR 1173 (1197) levels in H23 cells overexpressing PTPRH WT or various PTPRH deletions

Representation of the PTPRH domains and their location in the protein (A). The target region for deletion in each Δ construct is indicated by the blue bar. The table provides a complete description of the deletions and their position in the PTPRH protein. B) The generated constructs harboring deletions in either the PTPRH fibronectin3 domains or the phosphatase domain were aligned against the human PTPRH WT coding sequence. The red portions in the alignment represent the mismatch (deleted) regions. The arrows indicate positions where a single-nucleotide variation was found. Numbers represent the nucleotide position. C) Lung adenocarcinoma H23 (parental), H23 PTPRH KO, H23 PTPRH KO mock (control for lentivirus transduction), or H23 PTPRH KO cells in which PTPRH WT or various PTPRH deletions were added back to overexpress the protein were stimulated with EGF (100 ng/mL) for 15 min. The whole cell lysates (n=3/group) were used to immunoblot pEGFR 1173 (1197), EGFR, B-actin, PTPRH, and HA-tag and the representative blot is shown. Densitometry results for pEGFR 1173 (1197)/total EGFR ratio for the replicates are demonstrated as individual dots in the bar plot, and the mean +/- s.d. is shown. T-test was performed to compare each group with the parental cell (H23) and *$p<0.05$ was considered a significant result. Abbreviations: FN3 = fibronectin3; ns = non-significant; IB = immunoblot; nt = nucleotide

Figure 3. PTPRH does not coimmunoprecipitate with EGFR.

Cell lysates were immunoprecipitated (IP) for EGFR and immunoblotted (IB) for EGFR and PTPRH. Rabbit IgG antibody was used as a control isotype. A) Lung adenocarcinoma cells H23 or H23 PTPRH KO were stimulated with EGF (100 ng/mL) for 15 min. The whole cell lysate (WCL) of the colorectal cancer cell line HT29, which express high levels of PTPRH, was used as a positive control for IB, whereas H23 PTPRH KO cells were used as a negative control. B) H23 PTPRH KO cells in which PTPRH WT was added back were stimulated with EGF (100 ng/mL) at different time points (2, 5, 10, and 15 minutes) prior to cell lysis and IP. The same cell line was used for WCL positive control. Abbreviations: IB= immunoblot, IP= immunoprecipitation, m= minutes

Figure 4. Validation of lung adenocarcinoma cell lines expressing BioID2-only or PTPRH WT-BioID2.

H2023 and H23 PTPRH knockout cell lines transduced with BioID2-HA-only, PTPRH WT-BioID2-HA, or mock (control) were validated for expression of the constructs and their subcellular localization using immunoblot and immunofluorescence, respectively. A) Immunoblot against the HA-tag for mock (n=1/cell line), BioID2-only (n=2/cell line), and PTPRH WT-BioID2-HA (n=2/cell line) H2023 and H23 KO cells. Bands matching the correct molecular size for BioID2-HA and PTPRH WT-BioID2-HA are indicated by the arrows. B) Immunofluorescence was performed in all groups using antibodies against the HA-tag which are shown in magenta. DAPI staining is shown in blue. Representative cells showing localization of PTPRH WT-BioID2-HA in the plasma membrane and/or cytosol are indicated by arrows. Images are representative fields using 40x magnification, scale bar = 400 pixels. Abbreviations: ab = antibody; IB= immunoblot.

Figure 5. PTPRH interactors revealed by in vitro labeling technique (BioID) in lung adenocarcinoma cell lines.

H2023 and H23 PTPRH KO cell lines transduced with BioID2-HA-only, PTPRH WT-BioID2-HA, or mock (negative control) were serum starved for 24h, followed by stimulation with FBS and biotin for 18h. A) Immunoblot against biotin showing the presence of biotinylated proteins in the BioID2-only and PTPRH WT-BioID2-HA groups, with some bands (arrows) showing up exclusively in the PTPRH-WT-BioID2-HA groups. B) Venn diagram of biotinylated proteins identified in each PTPRH WT-BioID2-HA transduced cell line (n=1/cell line) by mass spectrometry. These proteins present a minimum of 3-fold increase in normalized total precursor intensity compared to their respective BioID2-only transduced cell line. C) Candidate PTPRH interactors (n=48) were screened for the presence of reported phospho sites in

the PhosphoSitePlus database. The percentage of proteins containing at least one pY or pS/pT sites are shown. D) STRING analysis of candidate PTPRH interactors (n=58). Abbreviations: IB = immunoblot; pY = phospho-Tyrosine; pS/pT = phospho-Serine/phospho-Threonine.

Figure 6. Transcriptome analysis of lung adenocarcinoma cell lines overexpressing PTPRH.

H2023 and H23 cell lines expressing endogenous or overexpressed PTPRH levels and H23 PTPRH knockout cells were serum starved for 24h, followed by stimulation with FBS for 16h prior to RNA extraction. A) PCA plot of counts normalized by variance stabilizing transformation (VST). B) Volcano plot of differentially expressed genes in the PTPRH overexpression cell lines compared to cell lines expressing endogenous PTPRH (parental cells) with padj < 0.05. Genes were considered upregulated (red) when log2 fold change > 2 and downregulated (blue) when log2 fold change < -2. C) Heatmap of top 30 most upregulated and downregulated differentially expressed genes (padj <0.05) in PTPRH overexpression cell lines. Log2 fold change (logFC), average expression (AveExpr), and Z-score for each gene are shown. Samples were clustered using hierarchical clustering analysis. D and E) GSEA plots showing significant enriched pathways in the PTPRH overexpression cell lines using the C6 oncogenic signature gene set (D) and the Hallmark gene set (E). F and H) Expression of differentially expressed protein tyrosine phosphatases (F) and tyrosine kinases (H) are represented as log10 normalized counts (padj <0.05).

Supplementary Figure. 1. PTPRH expression in lung adenocarcinoma cell lines.

Immunoblot against PTPRH in H23, H23 KO, H23 KO in which various PTPRH constructs (WT or harboring point mutations) were added back, A427, and HT-29 cell lines (A). HT-29 is a colorectal carcinoma cell line overexpressing endogeneous PTPRH and it was used as a positive control. None of the PTPRH point mutations addbacks were used for the purpose of this paper. B) Log2 fold change of PTPRH mRNA expression in A427 (used as a reference sample), H23, H23 KO, and HT-29 cells (n=3/cell line). Replicates are represented as individual dots in the bar plot, and the mean+/- s.d. is shown. C) Annotated map of the PTPRH WT- HA plasmid. D) H23 cells and two H23 PTPRH KO clones (#2 and #13) were screened for differences in pEGFR 1173 (1197) levels after 15 of EGF (100 ng/mL) stimulation by immunoblot (n=3/cell line). Results of densitometry for pEGFR 1173 (1197)/total EGFR ratio for the replicates are demonstrated as individual dots in the bar plots (mean +/- s.d.). T-test was performed to compare the PTPRH KO group with the parental cell (H23) and *p<0.05 was considered a significant result. Abbreviations: IB = immunoblot

Supplementary Figure 2. Subcellular localization of BioID2 constructs.

H2023 and H23 PTPRH knockout cell lines transduced with BioID2-HA-only, PTPRH WT-BioID2-HA, or mock (control) were stained with antibody against the BioID2 tag subcellular localization of protein is shown in green (immunofluorescence). DAPI staining is shown in blue. Representative cells showing localization of PTPRH WT-BioID2-HA in the plasma membrane and/or cytosol are indicated by arrows. Images are representative fields using 40x magnification, scale bar = 400 pixels. Abbreviations: ab = antibody.

Supplementary Fig. 3. Transcriptome analysis of lung adenocarcinoma cell lines overexpressing PTPRH.

Hierarchical clustering analysis of samples based on their normalized gene counts (rlog transformation)(A). B) Normalized enrichment score (NES) plot of AKT_UP.V1_UP and EGFR_UP.V1_UP gene sets in PTPRH overexpression cell lines. C) MA plot of log2 fold change and mean of normalized counts.

Fig 1: Investigation of pEGFR levels on H23 PTPRH knockout cells

A

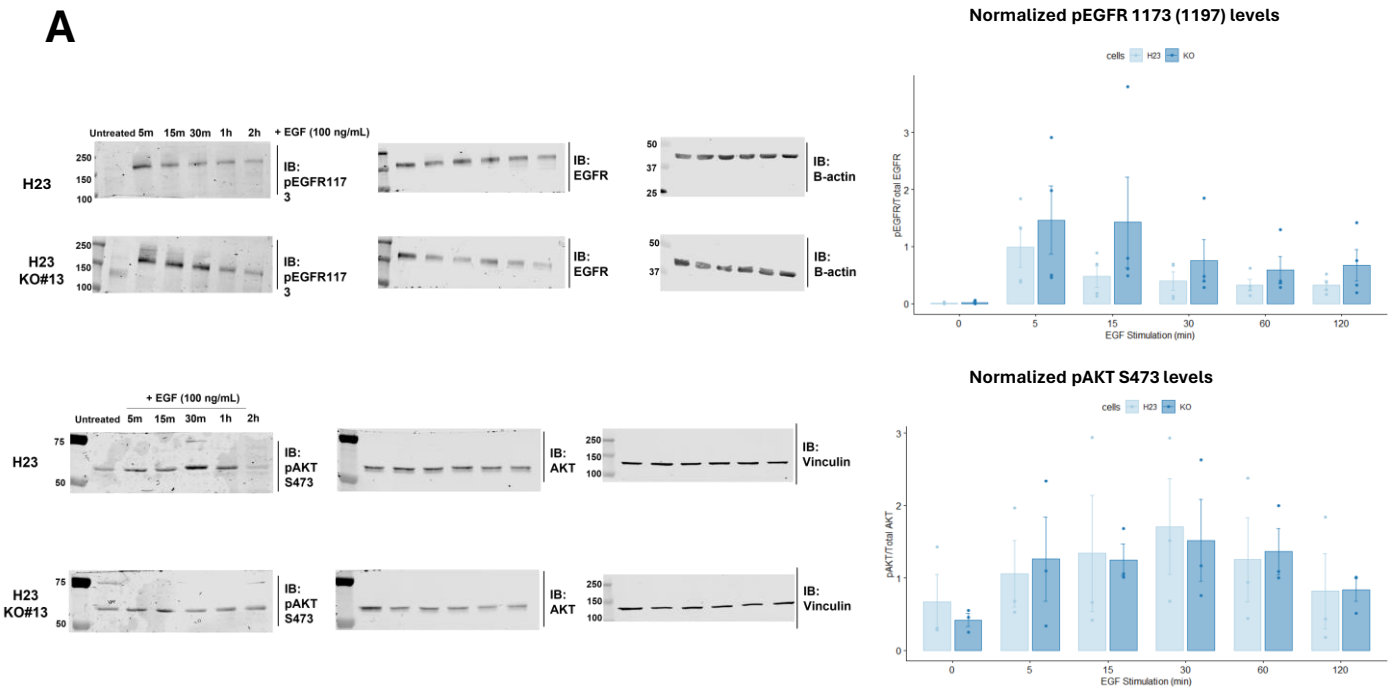

B

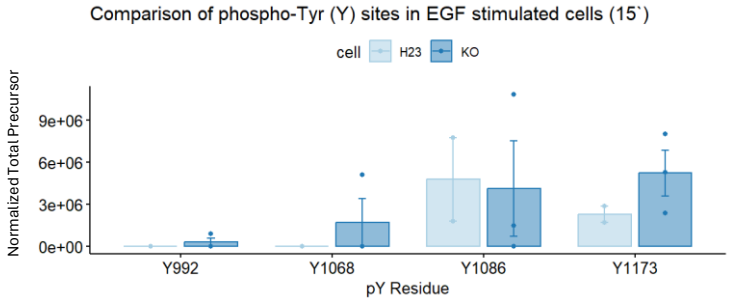

Peptide/Sample	KO #1	KO #2	KO #3	H23 #1	H23 #2
ALMDEEDMDDVVDADEYLIPQQGFFSS PSTSR (Y992)	871939.1	0	0	0	0
GSTAENAEYLR (Y1173)	2365493	5256077	8026998.2	1683354	2882294
RPAGSVQNPVYHNQPLNPAPSR (Y1086)	1490507	10848465	0	1768511	7758721
YSSDPTGALTEDSIDDTFLPVPEYINQSV PK (Y1068)	5076659	0	0	0	0

Fig 2: Investigation of pEGFR 1173 levels in H23 cells overexpressing PTPRH WT or various PTPRH deletions

A

Construct name	Description	Deletion Position
PTPRH-HA Δ1	Deletion of fibronectin3 domains 1 & 2	30 – 200 aa (90-600 nt)
PTPRH-HA Δ2	Deletion of fibronectin3 domains 3 & 4	209 – 364 aa (627-1092 nt)
PTPRH-HA Δ3	Deletion of fibronectin3 domains 5 & 6	396 – 556 aa (1188-1668 nt)
PTPRH-HA Δ4	Deletion of the end portion of the phosphatase domain	980 – 1080 aa (2940-3240 nt)

B

C

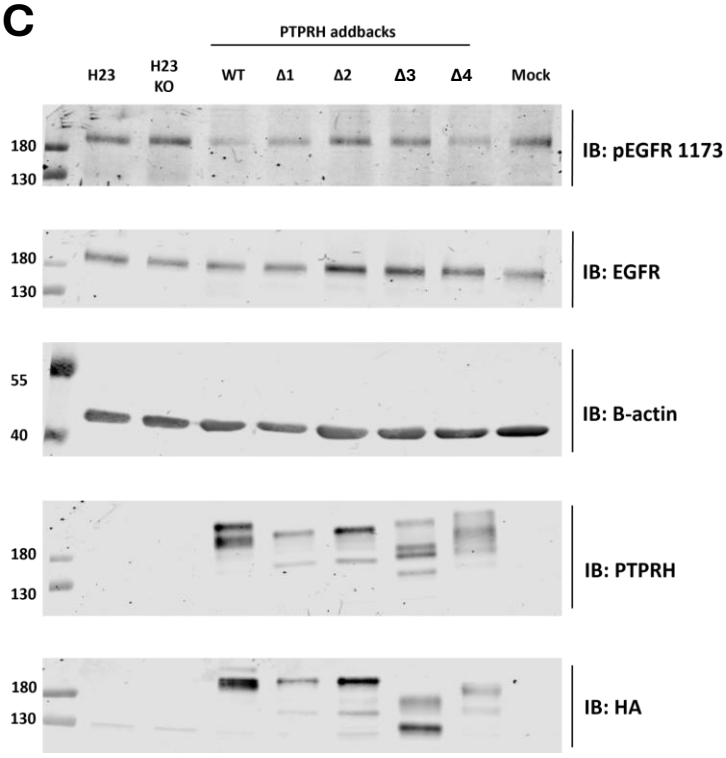

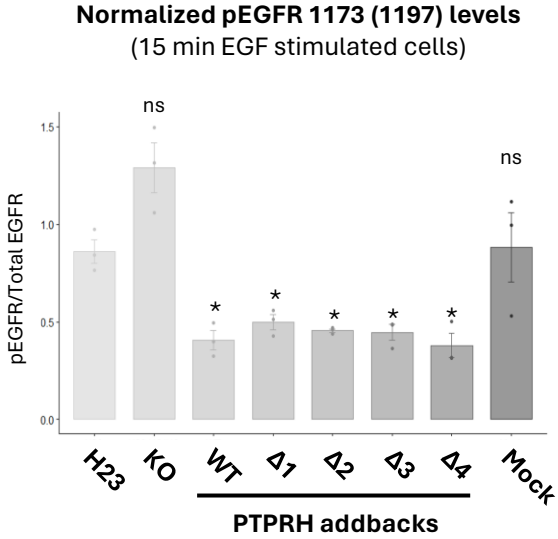

Fig 3: PTPRH does not co-immunoprecipitated with EGFR

A Cells were stimulated with EGF for 15 min

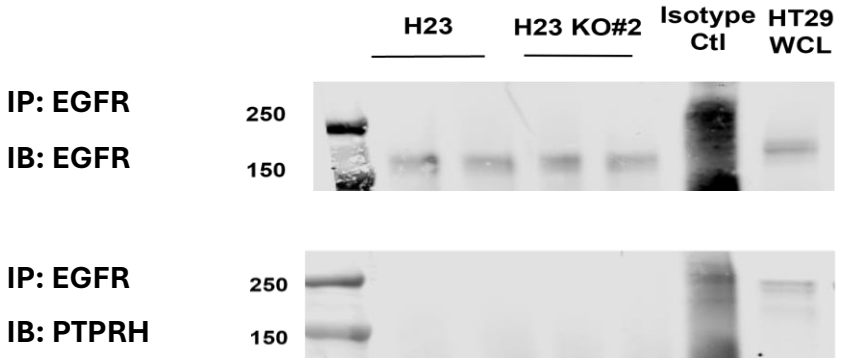

B PTPRH WT addback cells stimulated with EGF at different time points

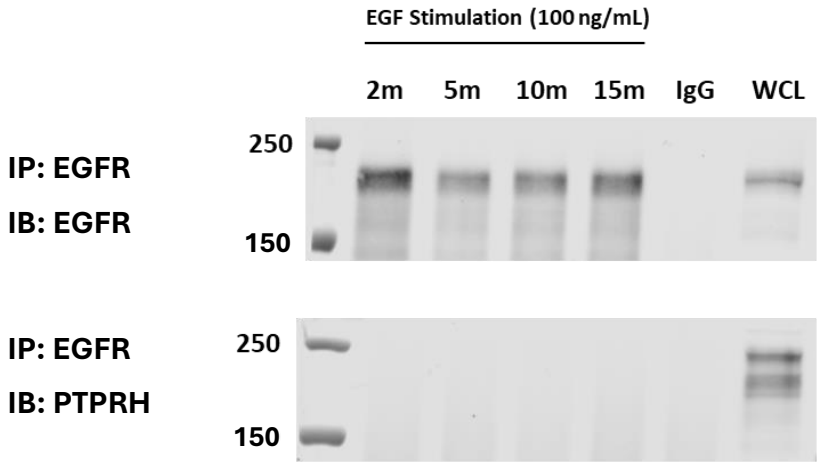

Fig 4: Validation of lung adenocarcinoma cell lines expressing BioID2-only or PTPRH WT-BioID2

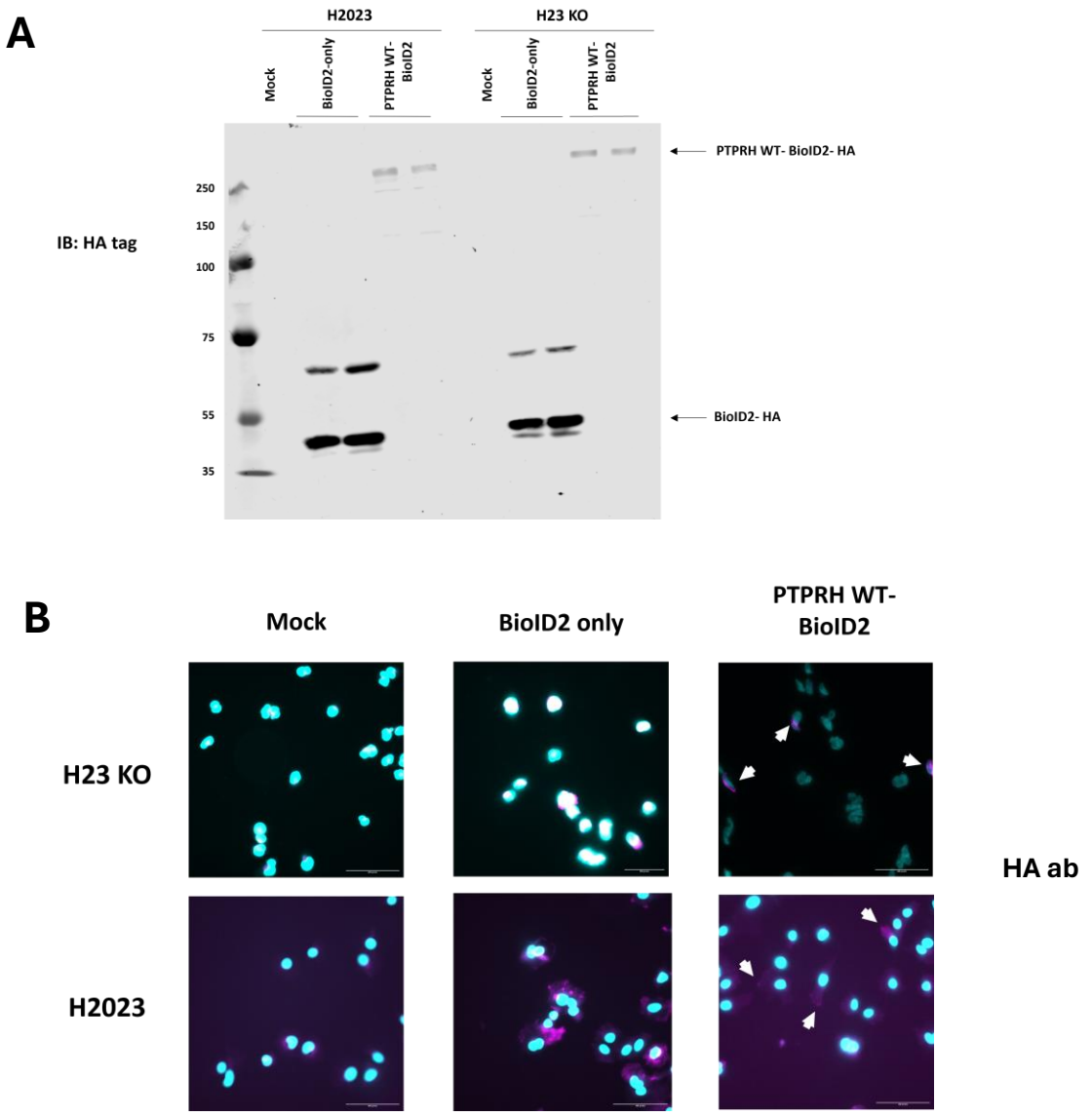

Fig 5: BioID reveals PTPRH interactors

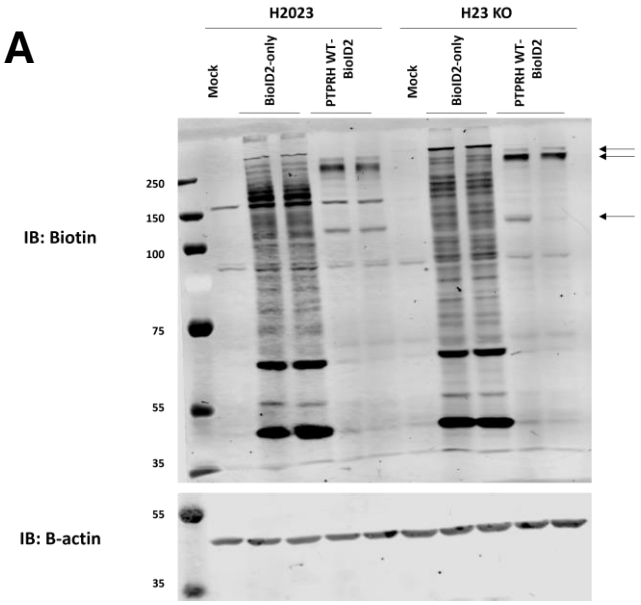

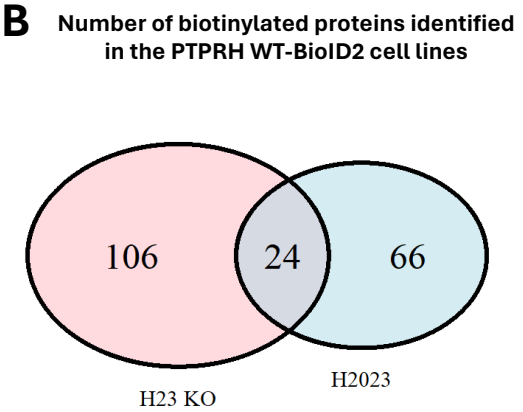

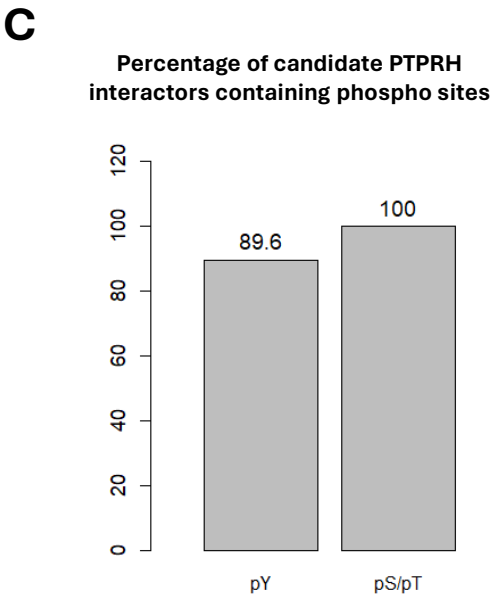

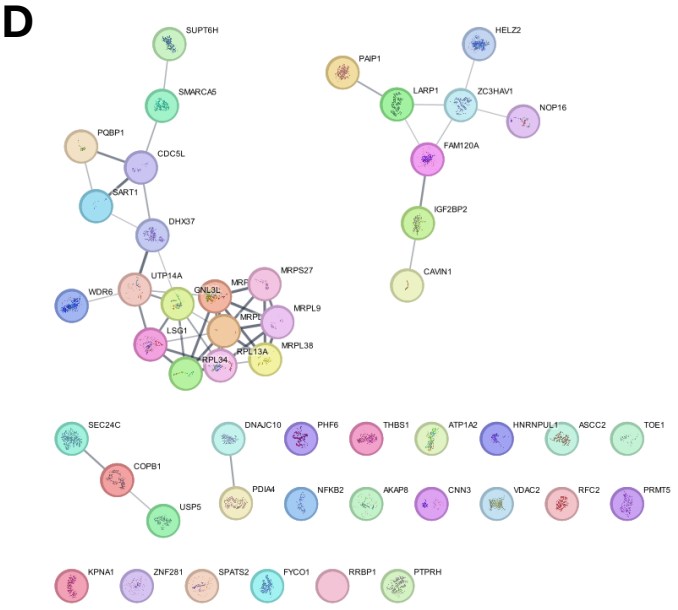

Fig 6: Transcriptome analysis of NSCLC cells overexpressing PTPRH

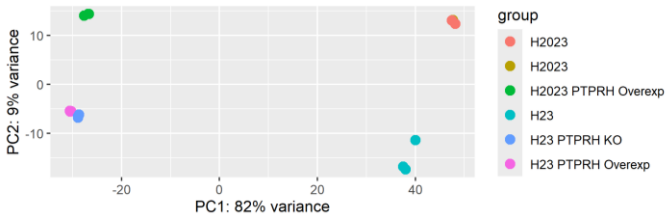

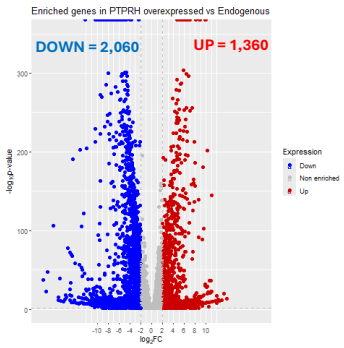

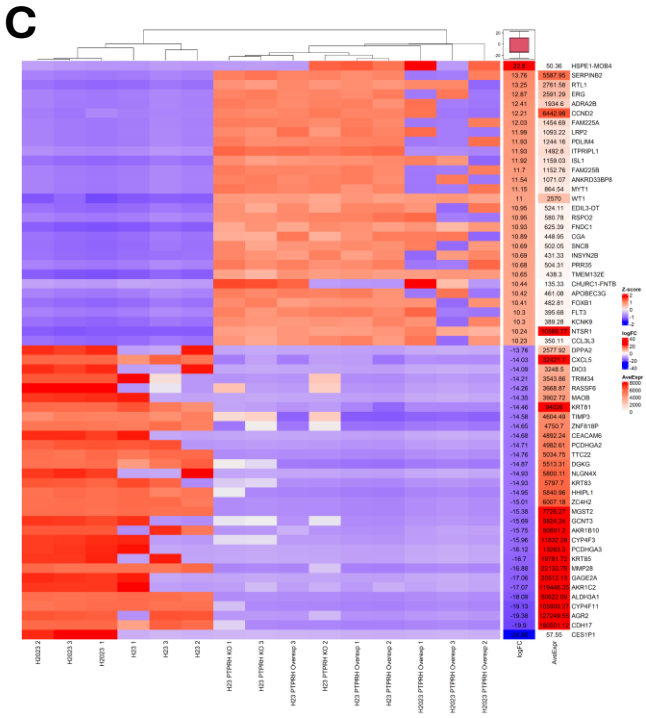

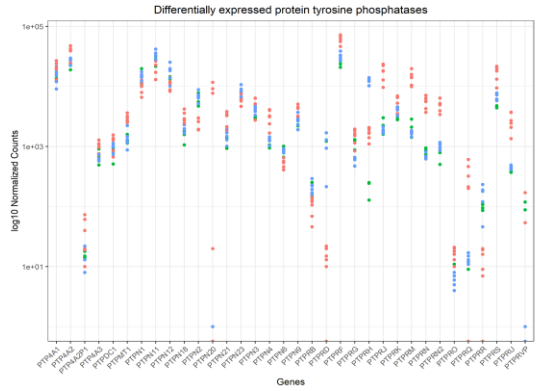

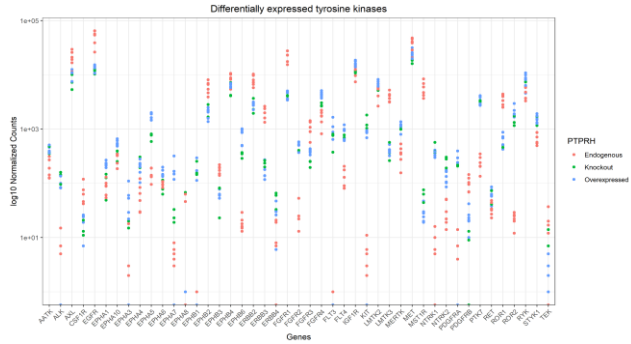

F Hallmark MSigDB

Pathway	NES	pval	padj
HALLMARK_ESTROGEN_RESPONSE_LATE	-1.83	$1.2 \cdot 10^{-4}$	$1.7 \cdot 10^{-3}$
HALLMARK_ESTROGEN_RESPONSE_EARLY	-1.81	$1.2 \cdot 10^{-4}$	$1.7 \cdot 10^{-3}$
HALLMARK_XENOBIOTIC_METABOLISM	-2.11	$1.3 \cdot 10^{-4}$	$1.7 \cdot 10^{-3}$
HALLMARK_INTERFERON_ALPHA_RESPONSE	-1.94	$1.3 \cdot 10^{-4}$	$1.7 \cdot 10^{-3}$
HALLMARK_INTERFERON_GAMMA_RESPONSE	-1.70	$2.4 \cdot 10^{-4}$	$2.4 \cdot 10^{-3}$
HALLMARK_APICAL_JUNCTION	-1.65	$4.9 \cdot 10^{-4}$	$3.9 \cdot 10^{-3}$
HALLMARK_E2F_TARGETS	1.93	$6.1 \cdot 10^{-4}$	$3.9 \cdot 10^{-3}$
HALLMARK_G2M_CHECKPOINT	1.69	$6.2 \cdot 10^{-4}$	$3.9 \cdot 10^{-3}$
HALLMARK_ADIPOGENESIS	-1.60	$1.8 \cdot 10^{-3}$	$1.0 \cdot 10^{-2}$
HALLMARK_FATTY_ACID_METABOLISM	-1.60	$2.9 \cdot 10^{-3}$	$1.5 \cdot 10^{-2}$
HALLMARK_WNT_BETA_CATENIN_SIGNALING	1.77	$3.6 \cdot 10^{-3}$	$1.6 \cdot 10^{-2}$
HALLMARK_COAGULATION	-1.59	$4.6 \cdot 10^{-3}$	$1.9 \cdot 10^{-2}$
HALLMARK_COMPLEMENT	-1.54	$5.7 \cdot 10^{-3}$	$2.2 \cdot 10^{-2}$
HALLMARK_REACTIVE_OXYGEN_SPECIES_PATHWAY	-1.67	$6.5 \cdot 10^{-3}$	$2.3 \cdot 10^{-2}$
HALLMARK_IL6_JAK_STAT3_SIGNALING	-1.60	$1.2 \cdot 10^{-2}$	$3.9 \cdot 10^{-2}$

G C6 MSigDB

Pathway	NES	pval	padj
NFE2L2.V2	-2.08	$1.1 \cdot 10^{-4}$	$5.8 \cdot 10^{-3}$
MEK_UP.V1_UP	-1.84	$1.2 \cdot 10^{-4}$	$5.8 \cdot 10^{-3}$
E2F1_UP.V1_DN	-1.75	$1.2 \cdot 10^{-4}$	$5.8 \cdot 10^{-3}$
LEF1_UP.V1_DN	-1.83	$1.2 \cdot 10^{-4}$	$5.8 \cdot 10^{-3}$
SINGH_KRAS_DEPENDENCY_SIGNATURE	-1.96	$1.6 \cdot 10^{-4}$	$6.1 \cdot 10^{-3}$
P53_DN.V1_DN	-1.77	$2.5 \cdot 10^{-4}$	$7.3 \cdot 10^{-3}$
CAHOY_ASTROGLIAL	-1.86	$2.8 \cdot 10^{-4}$	$7.3 \cdot 10^{-3}$
RAF_UP.V1_DN	-1.66	$4.8 \cdot 10^{-4}$	$1.0 \cdot 10^{-2}$
P53_DN.V1_UP	-1.70	$4.9 \cdot 10^{-4}$	$1.0 \cdot 10^{-2}$
ERBB2_UP.V1_UP	-1.64	$7.3 \cdot 10^{-4}$	$1.4 \cdot 10^{-2}$
IL21_UP.V1_DN	-1.69	$1.0 \cdot 10^{-3}$	$1.8 \cdot 10^{-2}$
LTE2_UP.V1_DN	-1.59	$1.4 \cdot 10^{-3}$	$2.2 \cdot 10^{-2}$
MEL18_DN.V1_UP	-1.64	$1.5 \cdot 10^{-3}$	$2.2 \cdot 10^{-2}$
BMI1_DN_MEL18_DN.V1_UP	-1.64	$1.7 \cdot 10^{-3}$	$2.2 \cdot 10^{-2}$
BMI1_DN.V1_UP	-1.61	$2.5 \cdot 10^{-3}$	$3.0 \cdot 10^{-2}$
LEF1_UP.V1_UP	1.53	$2.7 \cdot 10^{-3}$	$3.0 \cdot 10^{-2}$
KRAS.600.LUNG.BREAST_UP.V1_DN	-1.56	$2.7 \cdot 10^{-3}$	$3.0 \cdot 10^{-2}$
EGFR_UP.V1_UP	-1.55	$3.4 \cdot 10^{-3}$	$3.5 \cdot 10^{-2}$
EIF4E_DN	-1.65	$3.5 \cdot 10^{-3}$	$3.5 \cdot 10^{-2}$
LTE2_UP.V1_UP	-1.52	$5.0 \cdot 10^{-3}$	$4.5 \cdot 10^{-2}$
RPS14_DN.V1_UP	-1.56	$5.0 \cdot 10^{-3}$	$4.5 \cdot 10^{-2}$
MEK_UP.V1_DN	-1.52	$5.4 \cdot 10^{-3}$	$4.6 \cdot 10^{-2}$
AKT_UP.V1_UP	-1.53	$5.9 \cdot 10^{-3}$	$4.8 \cdot 10^{-2}$

S1: PTPRH and pEGFR 1173 expression in lung adenocarcinoma cell lines

A

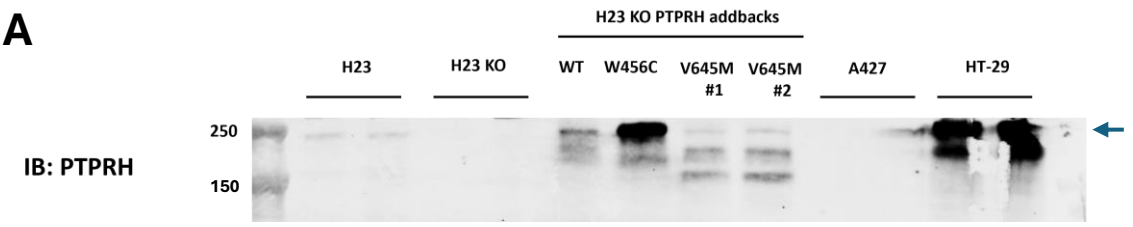

B

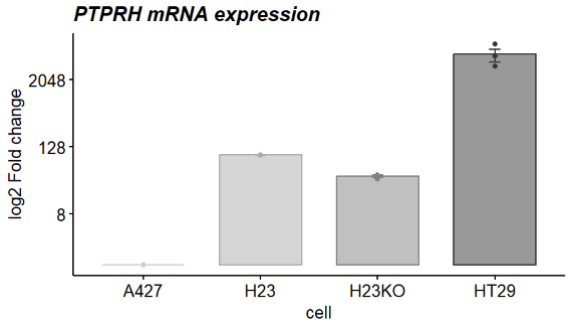

C

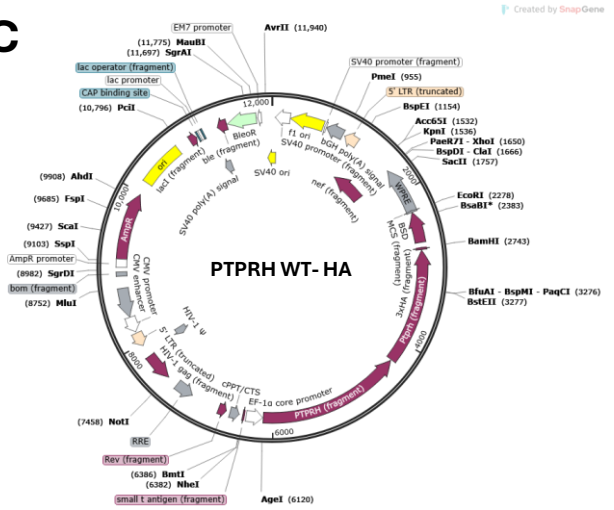

D

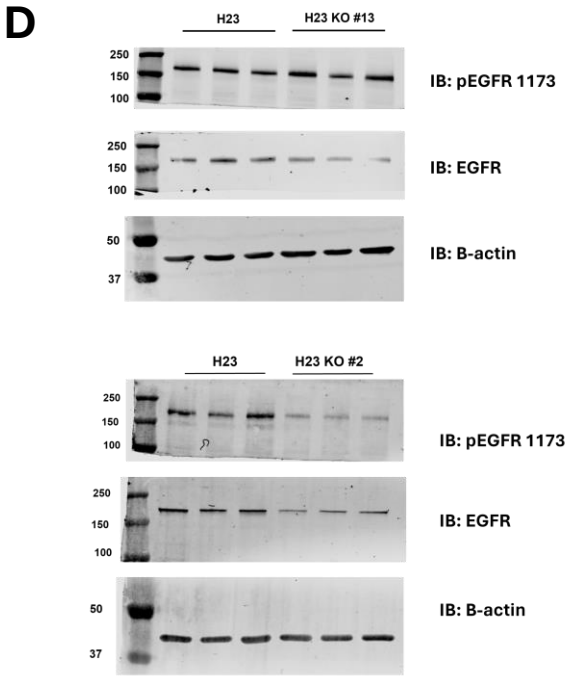

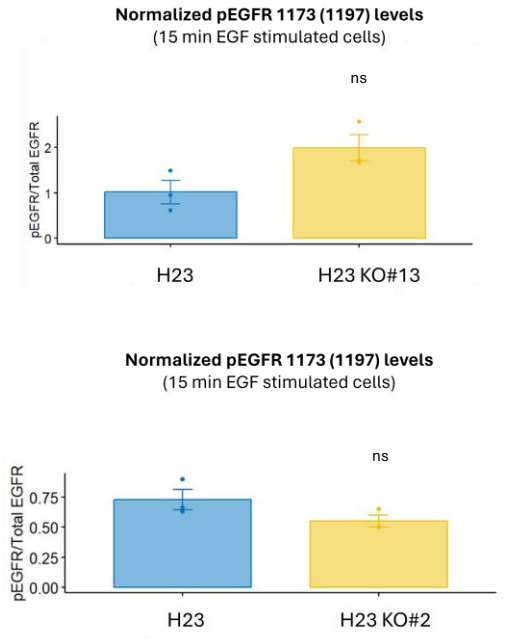

S2: Subcellular localization of BioID2 constructs

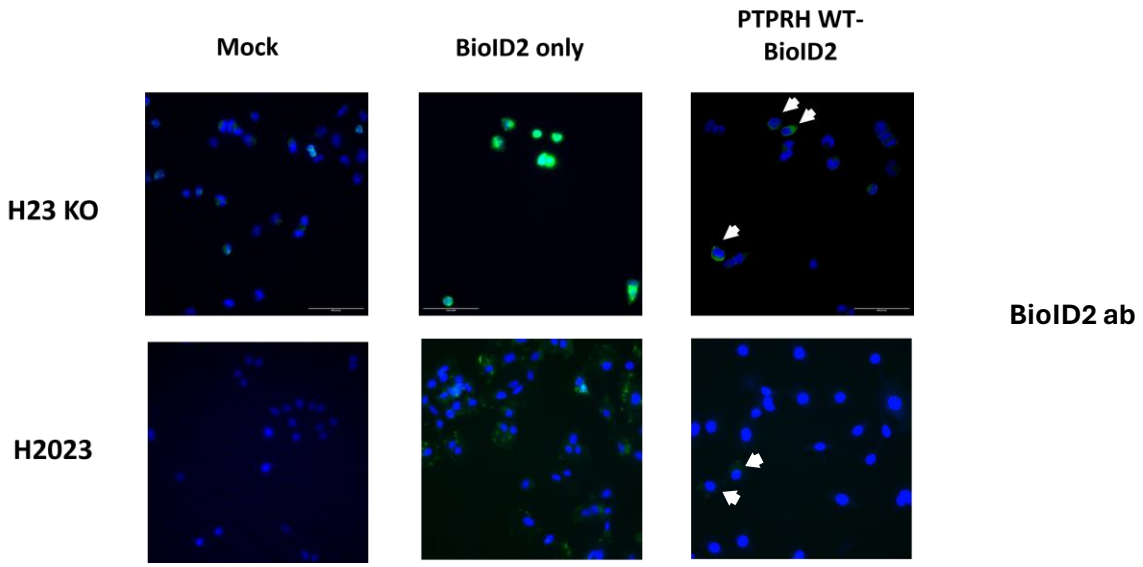

S3: RNA-seq results

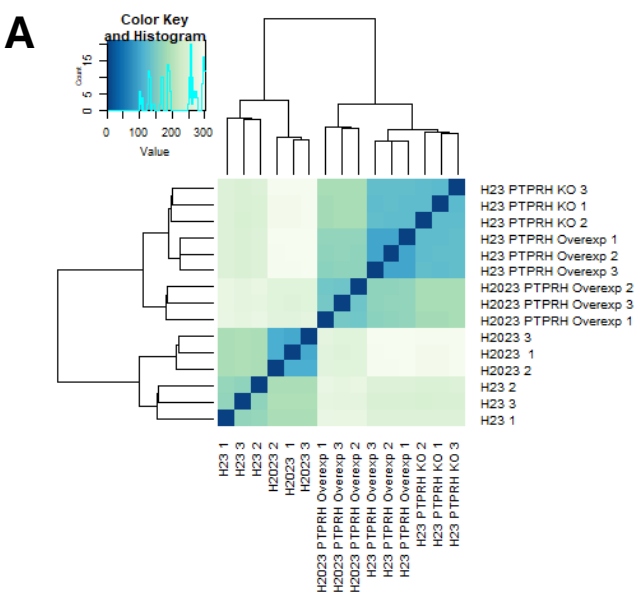

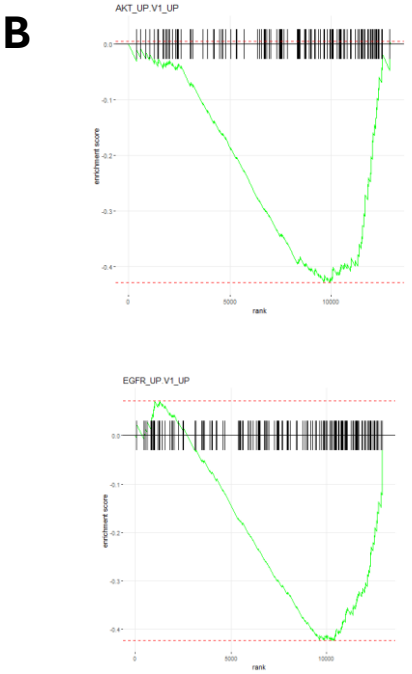

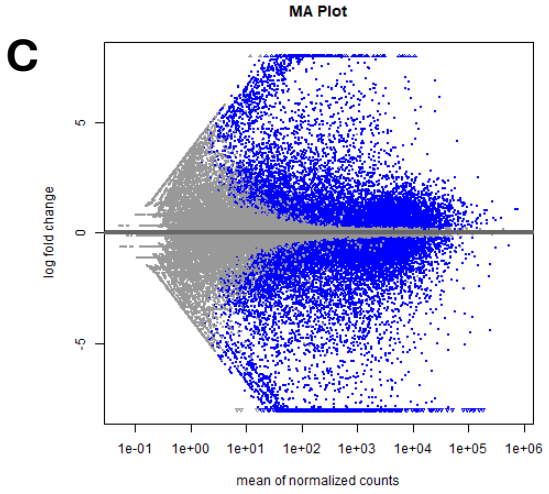

Figure legends

Figure 1. Investigation of pEGFR 1173 (1197) levels on H23 *PTPRH* knockout cell lines. Figure 1. Investigation of pEGFR 1173 (1197) levels on H23 *PTPRH* knockout cell lines. *A)* H23 and H23 *PTPRH* KO cells were stimulated with EGF (100 ng/mL) and cell lysates collected after 5, 15, 30, 60 and 120 minutes. Time point 0 represents non-stimulated (untreated) cells. Differences in pEGFR 1173 (1197) (*n*=4/group in each time point) and pAKT S473 (*n*=3/group in each time point) levels were assessed by immunoblot and representative blots are shown (mean +/- s.d.). Results of densitometry for pEGFR 1173 (1197)/total EGFR and pAKT/Total AKT ratio for the replicates are demonstrated as individual dots in the bar plots. T-test was performed to compare the PTPRH KO group with the parental cell (H23) in each time point and *p<0.05 was considered a significant result. *B)* EGFR was immunoprecipitated from H23 (n=2) and H23 PTPRH KO (n=3) cells stimulated with EGF (100 ng/mL) for 15 minutes and sent for mass spectrometry analysis. Quantitative values of normalized total precursor intensities for the identified phospho-Tyr sites in each cell line are represented in the table and the bar plot (mean +/- s.d.). Abbreviations: ns = non-significant; Tyr (Y) = tyrosine; IB = immunoblot

Figure 2. Investigating pEGFR 1173 (1197) levels in H23 cells overexpressing *PTPRH WT* or various *PTPRH* deletions . *A)* Representation of the PTPRH domains and their location in the protein. The target region for deletion in each Δ construct is indicated by the blue bar. The table provides a complete description of the deletions and their position in the PTPRH protein. *B)* The generated constructs harboring deletions in either the PTPRH fibronectin3 domains or the phosphatase domain were aligned against the human *PTPRH* WT coding sequence. The red portions in the alignment represent the mismatch (deleted) regions. The arrows indicate positions where a single-nucleotide variation was found. Numbers represent the nucleotide position. *C)* Lung adenocarcinoma H23 (parental), H23 PTPRH KO, H23 PTPRH KO mock (control for lentivirus transduction), or H23 PTPRH KO cells in which *PTPRH WT or* various PTPRH deletions were added back to overexpress the protein were stimulated with EGF (100 ng/mL) for 15 min. The whole cell lysates (*n*=3/group) were used to immunoblot pEGFR 1173 (1197), EGFR, B-actin, PTPRH, and HA-tag and the representative blot is shown. Densitometry results for pEGFR 1173 (1197)/total EGFR ratio for the replicates are demonstrated as individual dots in the bar plot, and the mean +/- s.d. is shown. T-test was performed to compare each group with the parental cell (H23) and *p<0.05 was considered a significant result. *Abbreviations:* FN3 = fibronectin3*;* ns = non-significant; IB = immunoblot; nt = nucleotide

Figure 3. PTPRH does not coimmunoprecipitate with EGFR. Cell lysates were immunoprecipitated (IP) for EGFR and immunoblotted (IB) for EGFR and PTPRH. Rabbit IgG antibody was used as a control isotype. *A)* Lung adenocarcinoma cells H23 or H23 *PTPRH* KO were stimulated with EGF (100 ng/mL) for 15 min. The whole cell lysate (WCL) of the colorectal cancer cell line HT29, which express high levels of PTPRH, was used as a positive control for IB, whereas H23 *PTPRH* KO cells were used as a negative control. B) H23 *PTPRH* KO cells in which *PTPRH* WT was added back were stimulated with EGF (100 ng/mL) at different time points (2, 5, 10, and 15 minutes) prior to cell lysis and IP. The same cell line was used for WCL positive control. *Abbreviations:* IB= immunoblot, IP= immunoprecipitation, m= minutes

Figure 4. Validation of lung adenocarcinoma cell lines expressing BioID2-only or PTPRH WT-BioID2. H2023 and H23 *PTPRH* knockout cell lines transduced with BioID2-HA-only, PTPRH WT-BioID2-HA, or mock (control) were validated for expression of the constructs and their subcellular localization using immunoblot and immunofluorescence, respectively. *A)* Immunoblot against the HA-tag for mock (n=1/cell line), BioID2-only (n=2/cell line), and PTPRH WT-BioID2-HA (n=2/cell line) H2023 and H23 KO cells. Bands matching the correct molecular size for BioID2-HA and PTPRH WT-BioID2-HA are indicated by the arrows. *B)* Immunofluorescence was performed in all groups using antibodies against the HA-tag which are shown in magenta. DAPI staining is shown in blue. Representative cells showing localization of PTPRH WT-BioID2-HA in the plasma membrane and/or cytosol are indicated by arrows. Images are representative fields using 40x magnification, scale bar = 400 pixels. *Abbreviations*: ab = antibody; IB= immunoblot.

Figure 5. PTPRH interactors revealed by *in vitro* labeling technique (BioID) in lung adenocarcinoma cell lines. H2023 and H23 *PTPRH* KO cell lines transduced with BioID2-HA-only, PTPRH WT-BioID2-HA, or mock (negative control) were serum starved for 24h, followed by stimulation with FBS and biotin for 18h. *A)* Immunoblot against biotin showing the presence of biotinylated proteins in the BioID2-only and PTPRH WT-BioID2-HA groups, with some bands (arrows) showing up exclusively in the PTPRH-WT-BioID2-HA groups. *B)* Venn diagram of biotinylated proteins identified in each PTPRH WT-BioID2-HA transduced cell line (n=1/cell line) by mass spectrometry. These proteins present a minimum of 3-fold increase in normalized total precursor intensity compared to their respective BioID2-only transduced cell line. *C)* Candidate PTPRH interactors (n=48) were screened for the presence of reported phospho sites in the PhosphoSitePlus database. The percentage of proteins containing at least one pY or pS/pT sites are shown. *D)* STRING analysis of candidate PTPRH interactors (n=58). *Abbreviations*: IB = immunoblot; pY = phospho-Tyrosine; pS/pT = phospho-Serine/phospho-Threonine.

Figure 6. Transcriptome analysis of lung adenocarcinoma cell lines overexpressing PTPRH. H2023 and H23 cell lines expressing endogenous or overexpressed PTPRH levels and H23 PTPRH knockout cells were serum starved for 24h, followed by stimulation with FBS for 16h prior to RNA extraction. *A)* PCA plot of counts normalized by variance stabilizing transformation (VST). *B)* Volcano plot of differentially expressed genes in the PTPRH overexpression cell lines compared to cell lines expressing endogenous PTPRH (parental cells) with padj < 0.05. Genes were considered upregulated (red) when log2 fold change > 2 and downregulated (blue) when log2 fold change < -2. *C)* Heatmap of top 30 most upregulated and downregulated differentially expressed genes (padj <0.05) in PTPRH overexpression cell lines. Log2 fold change (logFC), average expression (AveExpr), and Z-score for each gene are shown. Samples were clustered using hierarchical clustering analysis. *D* and *E)* GSEA plots showing significant enriched pathways in the PTPRH overexpression cell lines using the C6 oncogenic signature gene set *(D*) and the Hallmark gene set *(E). F and H)* Expression of differentially expressed protein tyrosine phosphatases *(F)* and tyrosine kinases *(H)* are represented as log10 normalized counts (padj <0.05).

Supplementary Figure. 1. PTPRH expression in lung adenocarcinoma cell lines. *A)* Immunoblot against PTPRH in H23, H23 KO, H23 KO in which various PTPRH constructs (WT or harboring point mutations) were added back, A427, and HT-29 cell lines. HT-29 is a colorectal carcinoma cell line overexpressing endogeneous PTPRH and it was used as a positive control. None of the PTPRH point mutations addbacks were used for the purpose of this paper. *B)* Log2 fold change of PTPRH mRNA expression in A427 (used as a reference sample), H23, H23 KO, and HT-29 cells (n=3/cell line). Replicates are represented as individual dots in the bar plot, and the mean+/- s.d. is shown. *C)* Annotated map of the PTPRH WT- HA plasmid. *D)* H23 cells and two *H23 PTPRH* KO clones (#2 and #13) were screened for differences in pEGFR 1173 (1197) levels after 15 of EGF (100 ng/mL) stimulation by immunoblot (n=3/cell line). Results of densitometry for pEGFR 1173 (1197)/total EGFR ratio for the replicates are demonstrated as individual dots in the bar plots (mean +/- s.d.). T-test was performed to compare the *PTPRH* KO group with the parental cell (H23) and *p<0.05 was considered a significant result. *Abbreviations:* IB = immunoblot

Supplementary Fig. 2. Subcellular localization of BioID2 constructs. H2023 and H23 *PTPRH* knockout cell lines transduced with BioID2-HA-only, PTPRH WT-BioID2-HA, or mock (control) were stained with antibody against the BioID2 tag subcellular localization of protein is shown in green (immunofluorescence). DAPI staining is shown in blue. Representative cells showing localization of PTPRH WT-BioID2-HA in the plasma membrane and/or cytosol are indicated by arrows. Images are representative fields using 40x magnification, scale bar = 400 pixels. *Abbreviations*: ab = antibody.

Supplementary Fig. 3. Transcriptome analysis of lung adenocarcinoma cell lines overexpressing PTPRH. *A)* Hierarchical clustering analysis of samples based on their normalized gene counts (rlog transformation). *B)* Normalized enrichment score (NES) plot of AKT_UP.V1_UP and EGFR_UP.V1_UP gene sets in PTPRH overexpression cell lines. *C)* MA plot of log2 fold change and mean of normalized counts.

Table 1: BioID reveals PTPRH interactors

		Quantitative Value (Normalized Total Precursor Intensity)	Quantitative Value (Normalized Total Precursor Intensity)	Quantitative Value (Normalized Total Precursor Intensity)	Quantitative Value (Normalized Total Precursor Intensity)
		H23 KO	**H2023**	**H23 KO**	**H2023**
Protein Symbol	**Fold Change**	**BioID2 only**	**BioID2 only**	**Ptprh WT-BioID2**	**Ptprh WT-BioID2**
PTPRH	31000	1,000.00	1,000.00	6.06E+07	871920
HELZ2	14000	1,000.00	1,000.00	2.36E+07	5124900
RFC2	9500	1,000.00	1,000.00	1.44E+07	4691200
NFKB2	5800	1,000.00	1,000.00	1.01E+07	1487200
USP5	5500	1,000.00	1,000.00	9755900	1158500
SPATS2	5400	1,000.00	1,000.00	5034300	5864400
ATP1A2	4800	1,000.00	1,000.00	1311200	8234700
WDR6	2800	1,000.00	1,000.00	1904300	3777100
SUPT6H	2700	1,000.00	1,000.00	2012000	3480600
COPB1	2700	1,000.00	1,000.00	2761500	2579500
PRMT5	1500	1,000.00	1,000.00	2869500	107760
PDIA4	41	481140	1,000.00	6297400	1.37E+07
AKAP8	29	1,000.00	352060	5302400	4772300
LSG1	19	1.28E+07	7727500	3.71E+08	9433600
CNN3	13	5439200	1.42E+07	2.99E+07	2.21E+08
DHX37	9.7	4029400	1213400	4.03E+07	1.06E+07
SART1	8.7	1086400	1,000.00	651720	8811600
THBS1	8.4	1.76E+07	1,000.00	3.73E+07	1.11E+08
PHF6	8.3	2246500	1,000.00	2879800	1.58E+07
RPL34	8.1	2.66E+07	1952200	2.23E+07	2.10E+08
VDAC2	6.4	482380	3684500	1.24E+07	1.43E+07
FYCO1	6.3	1,000.00	926450	2234900	3637900
MRPL38	6.3	6028600	1300600	1.49E+07	3.13E+07
ZNF281	5.4	1,000.00	3.47E+07	5751500	1.81E+08
MRPS27	5.2	1507600	3871500	2.36E+07	4327700
PQBP1	5.2	1,000.00	2385500	1036500	1.13E+07
HNRNPUL1	5	3.38E+07	5.32E+07	7.91E+07	3.54E+08
IGF2BP2	4.9	1,000.00	1.76E+07	2.56E+07	6.05E+07
ASCC2	4.4	865520	2313700	5818400	8264700
DNAJC10	4.4	1,000.00	770240	2283300	1127700
TOE1	4.4	718120	2353800	1083600	1.25E+07
MRPS11	4.2	5963500	3.03E+07	8832900	1.45E+08
CDC5L	4.2	2260700	259690	7347600	3155600
NOP16	4.1	1,000.00	3731700	4515300	1.07E+07
KPNA1	3.9	3612700	9510200	4.87E+07	2808100
SEC24C	3.9	4716800	2672000	3734500	2.51E+07
RPL13A	3.7	3.83E+08	1.57E+08	3.95E+08	1.60E+09
PAIP1	3.7	1,000.00	1236800	2883900	1659800
MRPL24	3.5	8644200	9022500	1.79E+07	4.47E+07
LARP1	3.5	1.29E+07	1.66E+07	3.84E+07	6.49E+07
GNL3L	3.5	2041600	3246000	5859900	1.26E+07
CAVIN1	3.5	5604100	6169300	1443700	3.95E+07
UTP14A	3.4	5249300	939310	1.16E+07	9676100
MRPL9	3.4	4820000	1.41E+07	2.89E+07	3.58E+07
SMARCA5	3.2	2434800	1,000.00	695170	7180700
RRBP1	3.2	2.19E+07	7.83E+07	1.26E+07	3.05E+08
ZC3HAV1	3.1	1701600	1.21E+08	2.83E+07	3.50E+08
FAM120A	3.1	1,000.00	5.54E+07	4680000	1.65E+08

Table 2: DAVID Functional Analysis (BioID)

Category	Term	Count	PValue	Fold Enrichment	Bonferroni	Benjamini	FDR
GOTERM_MF_DIRECT	GO:0003723~RNA binding	26	4.39E-16	6.934435	6.08E-14	6.01462E-14	5.97E-14
UP_KW_MOLECULAR_FUNCTION	KW-0687~Ribonucleoprotein	9	1.32E-06	10.31152	3.58E-05	3.57629E-05	3.44E-05
GOTERM_CC_DIRECT	GO:0005840~ribosome	7	2.74E-06	17.19911	0.000346	0.000345703	0.000332
UP_KW_MOLECULAR_FUNCTION	KW-0689~Ribosomal protein	7	1.19E-05	12.84848	0.000321	0.000160448	0.000155
UP_SEQ_FEATURE	CROSSLNK:Glycyl lysine isopeptide (Lys-Gly) (interchain with G-Cter in SUMO2)	13	2.14E-05	4.360904	0.009186	0.009228335	0.009228
UP_KW_PTM	KW-0007~Acetylation	24	2.69E-05	2.267113	0.000188	0.000215382	0.000215
GOTERM_CC_DIRECT	GO:0005654~nucleoplasm	22	6.66E-05	2.36794	0.008354	0.004194648	0.004028
GOTERM_BP_DIRECT	GO:0032543~mitochondrial translation	5	6.81E-05	22.26642	0.022345	0.022597354	0.022597
GOTERM_BP_DIRECT	GO:0006412~translation	6	0.000141	11.6821	0.045641	0.023355956	0.023356
UP_KW_PTM	KW-1017~Isopeptide bond	16	0.000168	2.835915	0.001178	0.000673753	0.000674
UP_KW_DOMAIN	KW-0677~Repeat	23	0.000175	1.951872	0.002101	0.002103445	0.002103
GOTERM_CC_DIRECT	GO:0005829~cytosol	25	0.000378	1.930291	0.046559	0.015889687	0.015259
UP_KW_BIOLOGICAL_PROCESS	KW-0810~Translation regulation	5	0.000597	12.37781	0.020685	0.020895794	0.020896
UP_KW_MOLECULAR_FUNCTION	KW-0694~RNA-binding	9	0.000678	4.299891	0.018151	0.006103994	0.005878
UP_KW_PTM	KW-0597~Phosphoprotein	35	0.002224	1.378406	0.015464	0.005587221	0.005587
UP_KW_PTM	KW-0832~Ubl conjugation	17	0.002794	2.095525	0.019392	0.005587221	0.005587

Table 3: GO Biological Processes (RNA-seq)

Upregulated GO	p.geomean	stat.mean	p.val	q.val	set.size	exp1
GO:0006281 DNA repair	9.24E-06	4.318077	9.24E-06	0.0398732	432	9.24E-06
GO:0008380 RNA splicing	2.22E-05	4.12196	2.22E-05	0.0398732	327	2.22E-05
GO:0051276 chromosome organization	2.32E-05	4.098638	2.32E-05	0.0398732	449	2.32E-05
GO:0006397 mRNA processing	3.50E-05	4.011524	3.50E-05	0.0430677	347	3.50E-05
GO:0022613 ribonucleoprotein complex biogenesis	4.18E-05	3.971604	4.18E-05	0.0430677	339	4.18E-05
GO:0051960 regulation of nervous system development	5.30E-05	3.901326	5.30E-05	0.0450794	319	5.30E-05
GO:0006338 chromatin remodeling	6.13E-05	3.863507	6.13E-05	0.0450794	413	6.13E-05
Downregulated GO						
GO:0032787 monocarboxylic acid metabolic process	8.11E-06	-4.339445	8.11E-06	0.0373209	386	8.11E-06
GO:0006631 fatty acid metabolic process	1.45E-05	-4.222542	1.45E-05	0.0373209	244	1.45E-05